Materials Today Nano 10 (2020) 100073

Contents lists available at ScienceDirect

Materials Today Nano

journal homepage: https://www.evise.com/profile/#/MTNANO/login

Multi-electron reactions of vanadium-based nanomaterials for high-capacity lithium batteries: challenges and opportunities

X. Xu, F. Xiong, J. Meng, Q. An, L. Mai*

State Key Laboratory of Advanced Technology for Materials Synthesis and Processing, Wuhan University of Technology, Wuhan, 430070, China

ARTICLE INFO

Article history:
Received 25 November 2019
Received in revised form
25 December 2019
Accepted 10 January 2020
Available online 18 January 2020

Keywords:
Multilithium reactions
High-capacity materials
Vanadium-based electrodes
Lithium storage

ABSTRACT

Achieving higher energy density is a very important target for the next-generation lithium-ion batteries (LIBs), which requires the innovation of electrode materials. Using multi-electron reaction electrodes for higher capacity is an effective approach to achieve the goal for higher energy density. Vanadium-based materials are an important group that can realize multi-electron reactions because of the rich valence variation of vanadium and have received great attention for high-capacity LIB electrodes through the history for battery researches in the past 40 years. In this review, we focus on the typical vanadium-based multi-electron reaction electrodes and discuss the structure/performance relationships, electrochemical mechanisms, issues, and optimization strategies, with emphasis on the challenges and opportunities of vanadium-based multi-electron reaction electrodes for next-generation LIBs.

1. Introduction

Lithium-ion battery (LIB) is one of the most important technologies for the social developing in the 21st century [1]. The application of LIBs in portable electronic devices, such as mobile phones and laptops, has greatly changed our lives. In recent years, the development of electric vehicles, which may reshape the energy landscape in the future, has attracted significant attentions [2]. The application of LIBs in electric vehicles results in a higher requirement for energy density of LIBs, which promotes the research wave for new electrode materials with new mechanism and new chemistry.

Higher energy density is the most important target for next-generation LIBs. A typical LIB cell is mainly composed of anode, cathode, separator, electrolyte, current collector, and housing [3,4]. During the working process, the insertion/extraction reaction of Li^+ in the electrodes occurs, and equal amounts of electrons are transferred through the external circuit [5]. The voltage gap between cathode and anode and the amount of Li^+ that can be stored by the electrodes (corresponding to capacity) are determinant for the energy density [6,7]. In the past decades, LIBs based on $LiCoO_2$//graphite system have achieved great success in commercialization. However, owing to the intrinsic capacity limitation (~137 mAh g^{-1} for $LiCoO_2$ and ~370 mAh g^{-1} for graphite), the energy density of a cell hardly exceeds 200 Wh kg^{-1} [8]. Increasing the energy density of a cell through decreasing the ratio of inactive components technically has reached the extremity. To meet the requirement of electric vehicles, doubling the energy density is the developing tendency in the future [9]. This goal determines that the present commercialized electrodes have to be replaced by new electrode systems. Using the multi-electron reaction electrodes to replace the conventional single electron redox system is an effective approach to improve the energy density. Multi-electron reaction means that multiple Li^+ insertion/extraction can be realized, thus delivering higher capacity and then higher energy density [10–12].

Among the large pool of electrode materials, vanadium-based electrodes are an important group which can realize multi-electron reactions and have attracted much attention in the past decades [13–15]. Note that the multivalent property of vanadium (such as V^{5+}, V^{4+}, V^{3+}, and V^{2+}) has generated great values for energy storage fields. For instance, the commercialized all-vanadium redox flow batteries are designed exactly based on the rich valence states of vanadium, where the V^{5+}/V^{4+} redox couple acts as catholyte and V^{3+}/V^{2+} redox couple as anolyte [16]. Also, the multivalent property of vanadium endows the vanadium-based electrodes with multi-electron reaction feature (Fig. 1). For example, V_2O_5 can realize 3 Li^+ insertion with a high theoretical specific capacity of ~440 mAh g^{-1}, when used as a lithium battery cathode [17]. Similarly, up to 3 Li^+ can be cycled in $Li_3V_2(PO_4)_3$, resulting in a high theoretical capacity of ~197 mAh g^{-1} among

* Corresponding author.
E-mail address: mlq518@whut.edu.cn (L. Mai).

https://doi.org/10.1016/j.mtnano.2020.100073
2588-8420/

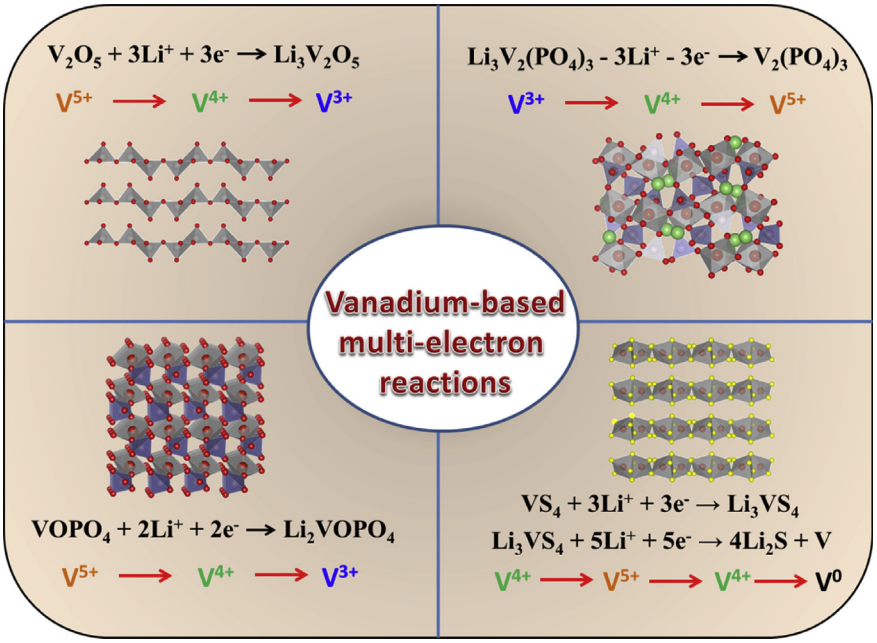

Fig. 1. Crystal structures, reaction formulas, and the vanadium valence evolutions of typical vanadium-based electrodes for multilithium reaction.

high-voltage phosphate LIB cathodes [18] (Fig. 1). However, challenge and opportunity coexists. In general, severe structural degradation and fast capacity fading will occur with multilithium intercalation.

In this review, we focus on the typical vanadium-based electrode materials with multi-electron reaction property and discuss their structures, reaction mechanisms, challenges, optimization strategies, and electrochemical performances for lithium batteries. We firstly look back the developing history of these typical vanadium-based lithium battery electrodes. Then, the vanadium-based multi-electron reaction cathodes and anodes are reviewed, respectively, with impressive progresses and important issues are emphasized. Finally, a summary and an outlook about the future direction are proposed. This review aims to provide a deeper understanding about the vanadium-based multi-electron reaction systems and give insights for the design of next-generation high-capacity lithium batteries.

2. History of vanadium-based electrodes for lithium batteries

The investigation of vanadium-based electrodes for lithium batteries can retrospect to 40 years ago. As early as 1976 [19], Whittingham has studied the Li^+ intercalation properties of V_2O_5. After that, many other kinds of vanadium-based materials were successively reported for their lithium storage properties. Notably, some important efforts were made based on vanadium-based electrodes at that period of time and finally led to the commercialization [20] (Fig. 2). Among them, silver vanadium oxides (SVOs) should be emphasized because their successful application as high energy cathode in primary (not rechargeable) batteries.

In the early 1980s, Li//SVO cell has been commercialized as a primary battery used for implantable cardiac defibrillators (ICDs) because of its high chemical stability and the ability to produce high current to power the ICDs. Keister et al. introduced the first implantable grade commercial cell in 1986, using $Ag_2V_4O_{11}$ as the cathode and lithium metal as the anode with a liquid organic electrolyte [20]. Soon afterwards, the superiority of $Ag_2V_4O_{11}$ among SVO as cathode was explored. It was found that $Ag_2V_4O_{11}$ delivered the highest capacity (theoretical value is 315 mAh g^{-1}), highest volumetric energy density, and lowest resistance compared with pristine V_2O_5 or other SVO cathodes with Ag/V ratios of 0.01–1.0 [21]. The details about the early investigation of SVO can be found in the review article by Takeuchi et al. in 2001 [20]. The discharge behavior (the lithium intercalation) of $Ag_2V_4O_{11}$ was demonstrated to be a multistep process. At the voltage of above 2.8 V, the lithium intercalation was believed to be companied by the reduction of Ag^+ to Ag. Upon the further lithium intercalation, the reduction of V^{5+} to V^{4+} and V^{4+} to V^{3+} will occur [22,23].

In the later years, investigations about battery electrodes mainly focused on two directions: one is how to further reduce the size and increase the energy density of lithium primary battery; the other is toward rechargeable batteries. The higher demands for lithium

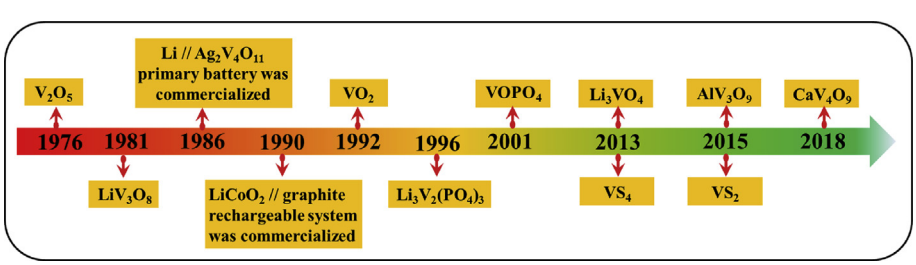

Fig. 2. A history outline of the development of vanadium-based multi-electron reaction electrodes for lithium batteries.

primary batteries push the research of new cathodes with higher capacity above 3.0 V (for higher energy density) or higher material density (for smaller battery size). Several new cathodes which were promising to achieve these goals were reported, such as $Ag_4V_2O_6F_2$ [24,25] and CuV_2O_6 [26] *etc*. A detailed review about these developments of SVO for lithium battery has been reported by Cheng and Chen in 2011 [27].

To achieve lithium rechargeable batteries, numerous endeavors were devoted to commercialize some systems with Li metal anode through the 1980s, such as Li//V_2O_5 battery with polymer electrolyte [1]. Even though being applied in a small niche market, the safety problem arising from the Li dendrites restricts the further growth of the battery systems with Li metal anode. In 1990, the $LiCoO_2$//graphite system was commercialized by Sony. This system, named 'lithium-ion battery' because of the absence of Li metal, achieved great success afterward and dominated the battery market until today. Even though the success of $LiCoO_2$//graphite system brings very significant impact on the research direction of battery electrodes, the research about vanadium-based electrode materials has never stopped (as shown in Fig. 2). Several different kinds of vanadium-based materials were successively reported for lithium storage in the following decade, such as VO_2, $Li_3V_2(PO_4)_3$, $VOPO_4$, etc. [13,18]. The research interests mainly originate from the high-capacity merit of these materials, even though some of them seems not good candidates for the commercialized 'lithium-ion battery' system because of the Li-poor property. New opportunities appeared recently for these high-capacity vanadium-based cathode materials, as the desire for higher energy density together with revived interests about Li-metal anode recently [28]. This trend inspired increased research attentions about the vanadium-based cathodes in recent years. Much improved electrochemical performance has been achieved through different optimization strategies [15,29]. And several new materials have been reported, such as AlV_3O_9, which shows a similar phase change and high capacity to V_2O_5 for Li^+ storage but displays a much better cycling stability than V_2O_5 [30]. Besides, the multi-electron reaction property also attracts much interest about vanadium-based materials on their application for high-capacity anodes to replace graphite. And several promising new anode materials were identified, such as Li_3VO_4 [31], VS_4 [32], VS_2 [33], CaV_4O_9 [34], etc., as shown in Fig. 2.

In the following sections, we will discuss the challenges and opportunities of the typical vanadium-based cathodes and anodes with multi-electron reactions for lithium batteries, with emphasis on the recent important progresses.

3. Vanadium-based multi-electron reaction cathodes

Owing to the multi-electron reaction property, vanadium-based cathode materials show great potential to overcome the capacity limitation of the current commercialized LIB cathodes, thus attracted much attention in the past years. Table 1 shows a comparison of the typical vanadium-based cathode materials for multilithium reaction. It is known that these vanadium-based cathodes can realize a double to triple capacity compared with commercialized LIB cathodes, but they also face different challenges, such as fast capacity fading or poor kinetics. In the following, we will give a detail discussion regarding their structures, electrochemical properties, challenges, and optimization strategies in the case of multilithium reaction.

3.1. V_2O_5

Since Whittingham reported the reversible electrochemical intercalation/deintercalation of Li^+ ions into V_2O_5 in 1976 [19], V_2O_5 has been considered as a promising cathode material for LIBs because of its easy synthesis, low cost, and high capacity. The typical layered crystal structure (Fig. 3a) [35] with interlayer spacing of ~4.37 Å endows V_2O_5 as a fascinating intercalation host for Li ions. The reaction mechanism of V_2O_5 as cathode for LIBs has been considered as multistep intercalation/deintercalation, which is described as [36–38]: $V_2O_5 + xLi^+ + xe^- \leftrightarrow Li_xV_2O_5$. The phases of ternary $Li_xV_2O_5$ are associated with the intercalated Li^+ amount (Fig. 3b). First, the α-$Li_xV_2O_5$ ($x < 0.01$) phase appears with trace amount of intercalated Li^+ ion, which converts to ε-$Li_xV_2O_5$ ($0.35 < x < 0.7$) phase with further lithiation. The intercalation of one Li^+ ion per formula results in the formation of δ-$Li_xV_2O_5$ ($x = 1$) phase. The phase transition from α to ε and ε to δ are both reversible. After that, the phase transforms to γ-$Li_xV_2O_5$ ($1 < x < 2$) with further lithium intercalation. As more than 2 Li^+ insertion, the phase transition from γ-$Li_xV_2O_5$ ($1 < x < 2$) to ω-$Li_xV_2O_5$ ($2 < x < 3$) with a tetragonal superstructure occurs. The structural framework of ω-$Li_xV_2O_5$ was demonstrated to be maintained, which undergoes a solid solution reaction in the subsequent lithium extraction process, as reflected by the sloping charge curve (Fig. 3b), indicating that the ω-$Li_xV_2O_5$ phase is irreversible [38]. Besides, the lithium diffusion coefficient was manifested to decrease significantly from 10^{-9} cm^2 s^{-1} for low lithium content to 10^{-12} cm^2 s^{-1} when three Li^+ intercalated [13]. Therefore, the electrochemical performance of V_2O_5 for Li storage is highly relevant to the voltage range, with a contradiction between capacity and cycling performance (Fig. 3c) [39]. As shown in Table 2, there are mainly three kinds of voltage ranges for the investigation of Li storage properties of V_2O_5, including 1.5–4.0 V (vs. Li^+/Li) for three Li^+ insertion, 2.0–4.0 V (vs. Li^+/Li) for two Li^+ insertion and 2.5–4.0 V (vs. Li^+/Li) for one Li^+ insertion (Fig. 3d–f). Although a high theoretical capacity (441 mAh g^{-1}) with three Li^+ intercalation can be achieved, the irreversible phase change and the decreased Li^+ diffusion kinetics upon three Li^+ intercalation will result in a fast capacity fading. Even though the irreversible phase change may unavoidable for three Li^+ intercalation, the Li^+ diffusion kinetics could be enhanced by certain strategies such as nanomaterials fabrication. Therefore, optimizing the cycling and rate performance of V_2O_5 in the case of multilithium intercalation has attracted great attentions.

In the past years, many strategies have been utilized to optimize V_2O_5 to improve the electrochemical performance for multiple Li^+ intercalation, such as nanostructure construction, conductive decoration, nanocomposite designing, and cation doping (Table 2). Here, we will briefly discuss these optimizing strategies and introduce some impressive results to shed light on the challenges and opportunities. A more detailed review about the relative reports can be found in the work by Yao et al. [17].

3.1.1. Nanostructured V_2O_5

Based on the equation $t = L^2/D$ (t represents the ion diffusion time, L represents the ion diffusion distance, and D represents the ion diffusion constant), synthesizing nanostructured electrode materials is an efficient approach to enhance the ion diffusion kinetics via shortening the diffusion distance. Moreover, the nanomaterials possess high specific surface area, which provide high electrode-electrolyte contact area and allow high Li^+ ion flux across the electrode-electrolyte interface.

For zero-dimensional (0D) nanostructured V_2O_5 (nanoparticles), the high surface energy leads to the great tendency of self-agglomeration during the cycling, resulting in the loss of specific surface area. In addition, the weak 'point to point' contacts among nanoparticles give rise to high interfacial resistances. Thus, V_2O_5 with one-dimensional (1D) structures have attracted a lot of attention because of its alleviated self-agglomeration tendency and 1D continuous electronic transport pathway. On the other hand, ultra-long 1D nanomaterials hold high promise to construct free-

Table 1
Comparison of the vanadium-based cathode materials for lithium batteries.

Materials	Theoretical specific capacity (mAh g^{-1})	Voltage plateaus (V)	Theoretical material density (g cm^{-3})	Advantages	Challenges
V_2O_5	147 (1 Li^+) 295 (2 Li^+) 441 (3 Li^+)	~3.4 ~3.15 ~2.25 ~1.85	3.37	1. Low cost 2. Simple fabrication 3. High capacity	Irreversible phase change and fast capacity fading
VO_2 (B)	161 (0.5 Li^+) 323 (1 Li^+) 485 (1.5 Li^+)	~2.5	4.04	1. Single redox couple 2. Good structure stability 3. High capacity	Mass production and ambiguous Li^+ storage mechanism
LiV_3O_8	279 (3 Li^+) 373 (4 Li^+)	~2.6	3.47	1. Good structural reversibility 2. High capacity	Poor electronic conductivity and Li^+ diffusion coefficient
ε-$VOPO_4$	166 (1 Li^+) 331 (2 Li^+)	~4.0 ~2.5	3.4	1. High voltage 2. High capacity	Poor kinetics and fast capacity fading
ε-$LiVOPO_4$	159 (1 Li^+) 317 (2 Li^+)	~4.0 ~2.5	3.27		
$Li_3V_2(PO_4)_3$	132 (2 Li^+) 197 (3 Li^+)	~4.05 ~3.66 ~3.58	2.88	1. High voltage 2. High thermal stability 3. Fast Li diffusion coefficient	Inferior cycling and rate performance in the case of three lithium reaction

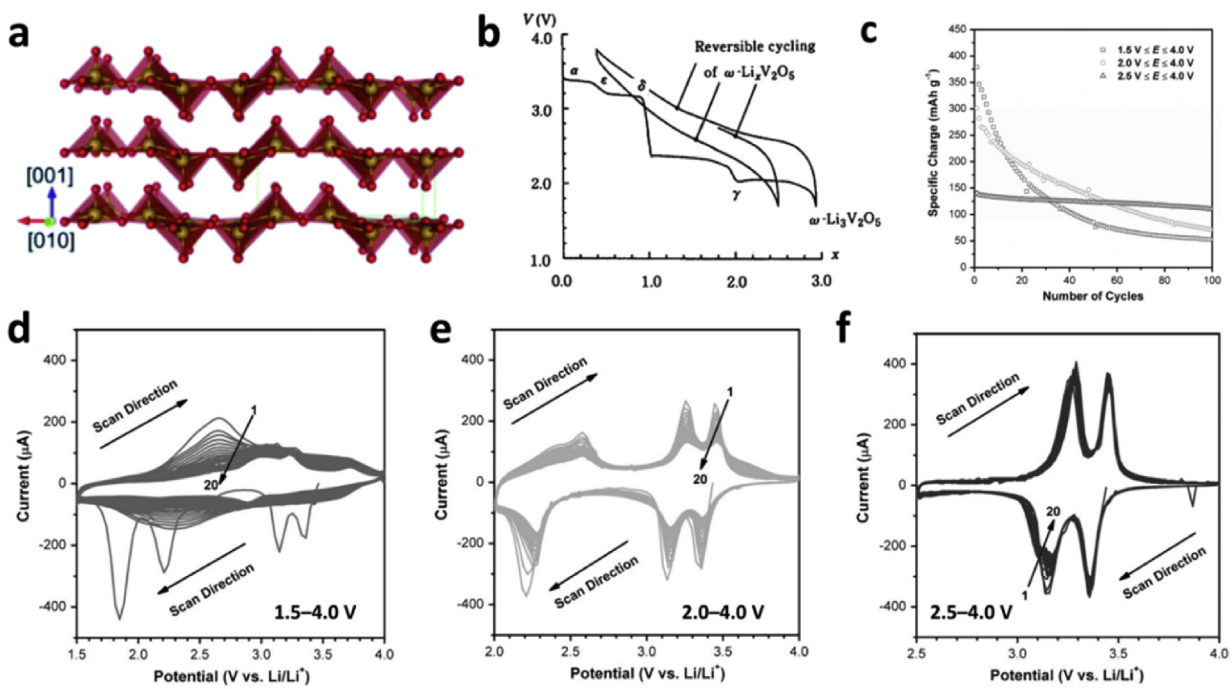

Fig. 3. (a) The crystal structure of orthorhombic V_2O_5. (b) The charge/discharge curves of orthorhombic V_2O_5. (c) The cycling performances of V_2O_5 at different potential ranges. (d–f) Cyclic voltammetry curves for 20 cycles of orthorhombic V_2O_5 at potential range of 1.5–4.0 V (d), 2.0–4.0 V (e), and 2.5–4.0 V (f), respectively. Reproduced with permission from (a) The Royal Society of Chemistry [35], (b) Elsevier [38] and (c–f) The Royal Society of Chemistry [39].

standing electrodes (Fig. 4a) for flexible devices (Fig. 4b) [44]. Recently, two-dimensional (2D) nanostructures also attract great attention in energy storage field. For LIB electrodes, the large surface area and ultra-thin thickness of 2D nanostructures are beneficial for Li^+ ion diffusion. Numerous 2D V_2O_5 nanomaterials with excellent electrochemical performance have been reported [42,47,49,104]. However, compared with bulk materials, the low tap density of 1D and 2D nanomaterials reduces the volumetric energy density, which is not beneficial for its practical application. Constructing nanostructure-assembled three-dimensional (3D) hierarchical microstructures is an efficient strategy to both increase the tap density and maintain the advantages of nanostructure [51–53,55,56,105]. For example, Zhang et al. [51] reported the V_2O_5 hollow microclews formed from the self-rolling of nanowires, which display a similar initial capacity to that of V_2O_5 nanowires. However, the tap density of V_2O_5 hollow microclews is about 2.3 times of that of V_2O_5 nanowires.

Besides, the structures with nanosized pores have also been proposed to enhance the electrochemical performance of V_2O_5 [57,59,65,67,70,105–109]. The porous structures or hollow structures not only improve the specific surface area but also provide space to accommodate the volume change during the multiple Li^+

Table 2
The Li-storage performance of partial orthorhombic V_2O_5-based cathode materials.

Materials	Potential window (V vs. Li^+/Li)	Maximal capacity (mAh g^{-1}/mA g^{-1})	Cycling performance	Reference
V_2O_5 nanorods	2.0–4.0	256/147	90.2%/30 cycles	[40]
Ultralong hierarchical V_2O_5 nanowires	1.75–4.0	390/30	51.5%/50 cycles	[41]
	2.0–4.0	275/30	68%/50 cycles	
Ultrathin V_2O_5 nanosheets	2.4–4.0	146/147	100%/200 cycles	[42]
Centimeter-long V_2O_5 nanowires	1.5–4.0	351/50	49.9%/20 cycles	[43]
V_2O_5/multi-walled carbon nanotube (MWCNT) free-standing film	2.5–4.0	~149/25	~96.0%/50 cycles	[44]
V_2O_5@TiO_2 core–shell nanoplatelets	2.0–4.0	255/60	75.8%/100 cycles	[45]
V_2O_5 nanobelt arrays	2.0–4.0	146/73.5	97%/100 cycles	[46]
Ultra-large V_2O_5 nanosheets	2.5–4.0	141/100	93.8%/200 cycles	[47]
V_2O_5 nanobelts	2.0–4.0	281/59	86%/50 cycles	[48]
Ultrathin V_2O_5 nanosheets	2.0–4.0	292/59	93.8%/50 cycles	[49]
V_2O_5 nanobelt arrays	2.0–4.0	298/100	97.0%/50 cycles	[50]
V_2O_5 hollow microclew	2.4–4.0	146.8/100	94.4%50 cycles	[51]
Nanorod-assembled V_2O_5 microflowers	2.0–4.0	274/300	79.9%/50 cycles	[52]
V_2O_5 nanosheet-assembled hollow microflowers	2.0–4.0	284/300	74.3%/50 cycles	[53]
	2.5–4.0	140/300	86.1%/50 cycles	
V_2O_5 nanosheet-assembled microspheres	2.0–4.0	300/30	74.2%/250 cycles	[54]
Hierarchical V_2O_5 microflowers	2.5–4.0	145/200	74.1%/3000 cycles	[55]
V_2O_5 interconnected microspheres	2.0–4.0	280/294	81%/200 cycles	[56]
Three-dimensional porous V_2O_5 hierarchical microplates	2.4–4.0	146/100	98.2%/100 cycles	[57]
Nanoflakes-assembled three-dimensional hollow-porous V_2O_5 microspheres	2.0–4.0	283/100	80.2%/200 cycles	[58]
Three-dimensional porous V_2O_5 hierarchical octahedrons	2.4–4.0	141/100	96.9%/500 cycles	[59]
Three-dimensional interconnected V_2O_5 nanonetwork	2.4–4.0	149/100	98.8%/1000 cycles	[60]
Rattle-type V_2O_5 hollow microspheres	2.0–4.0	291/100	64.5%/100 cycles	[61]
Yolk–shell V_2O_5	2.0–4.0	275/300	79%/100 cycles	[62]
Mesoporous single-crystalline V_2O_5 nanorods assembled hollow microspheres	2.5–4.0	145.8/73.5	90%/200 cycles	[63]
Three-dimensional porous V_2O_5 thin films	2.5–4.0	142/73.5	~100%/200 cycles	[64]
Three-dimensional porous V_2O_5 hierarchical microspheres	2.5–4.0	140.3/75	89.3%/100 cycles	[65]
V_2O_5 hollow nanospheres	2.0–4.0	292/100	92.6%/50 cycles	[66]
Mesoporous V_2O_5 nanosheets	2.5–4.0	147/100	91.0%/1000 cycles	[67]
Three-dimensional continuous multilayer V_2O_5 hollow sphere arrays	2.0–4.0	293/147	79.2%/300 cycles	[68]
Yolk–shell V_2O_5	2.0–4.0	271/1000	74.2%/100 cycles	[69]
Porous V_2O_5 cuboids	2.5–4.0	143/73.5	89.3%/400 cycles	[70]
Tripe-shelled V_2O_5 hollow spheres	1.5–4.0	565.4/50	89.8%/100 cycles	[71]
Carbon-coated V_2O_5 nanocrystals	2.0–4.0	297/1000	97.3%/50 cycles	[72]
Carbon cloth supported V_2O_5 nanoflake arrays	2.0–4.0	292/150	94.0%/100 cycles	[73]
V_2O_5/mesoporous carbon composite	2.0–4.0	291/100	56%/100 cycles	[74]
V_2O_5 quantum dots/graphene nanocomposite	2.0–4.0	245/100	84.7%/300 cycles	[75]
V_2O_5 nanocrystals on reduced graphene-oxide balls	2.0–4.0	282/1000	75.9%/100 cycles	[76]
Ultralong single crystalline V_2O_5 nanowire/graphene composite	1.5–4.0	412/50	~34.8%/100 cycles	[77]
V_2O_5 nanosheets/reduced graphene oxide hierarchical nanocomposite	2.0–4.0	271/60	52%/160 cycles	[78]
V_2O_5 nanorods/graphene	2.0–4.0	235/20	72.8%/100 cycles	[79]
Reduced graphene oxide supported highly porous V_2O_5 spheres	2.0–4.0	238/90	85.0%/50 cycles	[80]
Reduced graphene oxide enwrapped V_2O_5 nanorods	2.5–4.0	146/150	95.4%/100 cycles	[81]
	2.0–4.0	287/100	72.1%/50 cycles	
Crumpled rGO encapsulated hollow V_2O_5 nano/microsphere	2.0–4.0	291/100	94%/200 cycles	[82]
Interconnected V_2O_5 nanosheets assembled on CNT	2.0–4.0	285/300	91.3%/400 cycles	[83]
V_2O_5 nanosheets encapsulated within multigraphitic nanotubes	2.0–4.0	224/30	91.7%/200 cycles	[84]
TiO_2 coated amorphous V_2O_5/carbon nanotube paper	1.5–4.0	397/100	~87.0%/100 cycles	[85]
Porous sheet–like V_2O_5–CNT nanocomposite	2.0–4.0	350/60	71.0%/300 cycles	[86]
V_2O_5/single-walled carbon nanotube (SWCNT) hybrid mesoporous films	2.0–4.0	~590/300	94%/40 cycles	[87]
Bowknot-like RuO_2 quantum dots@V_2O_5	2.0–4.0	~260/100	87%/100 cycles	[88]
Three-dimensional V_2O_5/NaV_6O_{15} hierarchical heterostructures	2.4–4.0	~145/100	92%/1000 cycles	[89]
SnO_2/V_2O_5 core/shell nanowires	2.7–4.0	138/200	93%/500 cycles	[90]
TiO_2-coated V_2O_5 nanorods	1.7–4.0	330.6/30	76%/60 cycles	[91]
Ag nanoparticles and TiO_2 nanorods on V_2O_5 nanosheets	1.5–4.0	442/100	38.5%/100 cycles	[92]
SiO_2-coated V_2O_5 nanoflake arrays	2.0–4.0	289/100	96.9%/100 cycles	[93]
Cucumber-like V_2O_5/PEDOT&MnO_2 nanowires	2.0–4.0	185/50	70.7%/200 cycles	[94]
V_2O_5/PEDOT core/shell nanobelt array on three-dimensional graphite foam	2.0–4.0	297/300	98%/1000 cycles	[95]
V_2O_5–PPy films	1.5–4.0	313/40	60.1%/100 cycles	[96]
Hydrogenated V_2O_5 nanosheets	2.0–4.0	259/100	81.1%/200 cycles	[97]
Mn-doped V_2O_5 nanoflakes	2.0–4.0	253/300	79.4%/50 cycles	[98]
Al-doped V_2O_5/rGO nanocomposite	2.0–4.0	274/300	90.1%/50 cycles	[99]
Carbon-encapsulated Mn-doped V_2O_5 nanorods	2.0–4.0	265/29.4	94%/500 cycles	[100]
Ni-doped hierarchical V_2O_5 hollow microspheres	2.0–4.0	294/50	91%/50 cycles	[101]
Self-doped V^{4+}–V_2O_5 nanoflakes	2.0–4.0	293/100	89%/100 cycles	[102]
Cu doped V_2O_5 flowers	2.01–4.0	266/58.8	85%/50 cycles	[103]

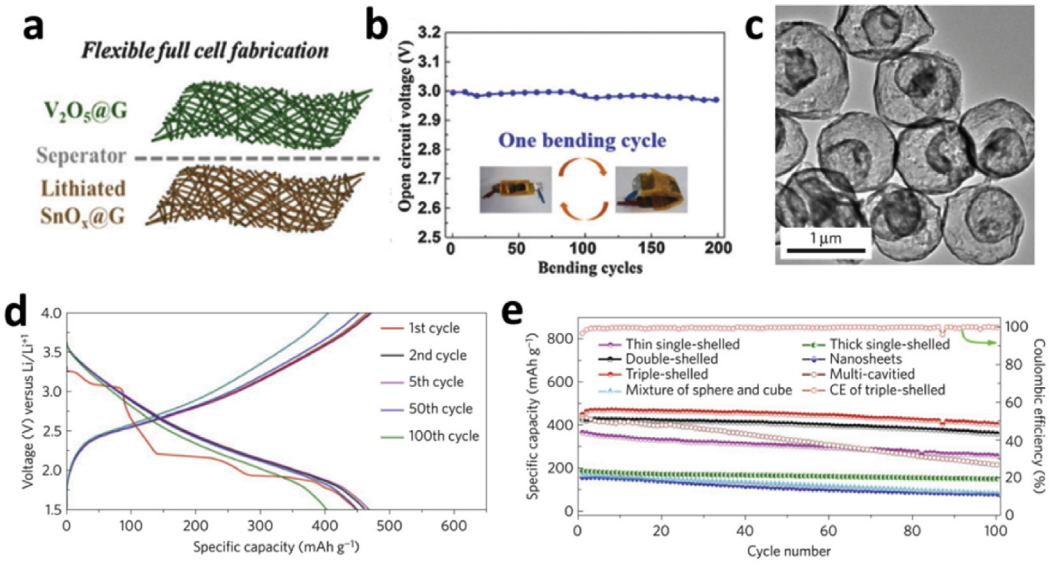

Fig. 4. (a) The schematic illustration of the fabrication of a flexible Sn-V_2O_5 battery. (b) The open circuit voltage of flexible Sn-V_2O_5 battery over 200 bending cycles. (c) SEM image of the triple-shelled hollow porous V_2O_5 microspheres. (d) Charge/discharge profiles of the triple-shelled hollow porous V_2O_5 microspheres after different cycles at 1000 mA g^{-1}. (e) Cycling performance of porous V_2O_5 microspheres at 1000 mA g^{-1}. Reproduced with permission from (a–b) The Royal Society of Chemistry [84] and (c–e) Nature Publishing Group [71]. SEM, scanning electron microscopy.

ion intercalation/deintercalation. Moreover, high porosity is beneficial for the electrolyte permeation and Li^+ ion transportation. Therefore, the 3D hollow V_2O_5 microspheres were demonstrated to exhibit excellent Li storage performance. Wang et al. [71] presented the multishelled hollow porous V_2O_5 microspheres synthesized via an anion-adsorption mechanism. The triple-shelled hollow porous V_2O_5 microspheres (3S-V_2O_5-HMSs) (Fig. 4c) exhibit the highest capacity of 565.4 mAh g^{-1} at 50 mA g^{-1} in 1.5–4.0 V, which exceeds the theoretical value of V_2O_5. The authors demonstrated that the exceeded capacity comes from the capacitive-controlled capacity. Even at 2000 mA g^{-1}, the capacity of 3S-V_2O_5-HMSs still remains 331.8 mAh g^{-1}. Moreover, a capacity of 402.4 mAh g^{-1} was obtained after 100 cycles at 1000 mA g^{-1} with only 0.10% loss per cycle (Fig. 4d and e). The outstanding electrochemical performance of 3S-V_2O_5-HMSs is because of (1) large specific surface area and pore volume, which increases Li^+ storage sites and facilitates electrolyte penetration and (2) the thin porous shells, which provides short Li^+ ion diffusion pathways and greatly increases the Li^+ diffusion kinetics.

3.1.2. V_2O_5-based nanocomposites

Nanocomposites combine the advantages of different materials to counteract the individual drawbacks. V_2O_5 has a layered structure with high theoretical capacity for Li^+ ion intercalation/deintercalation but suffers from poor electrical conductivity and fast capacity fading. Thus, compositing with conductive materials to make up for the disadvantages of V_2O_5 is a promising strategy to improve the electrochemical performance. V_2O_5-based nanocomposites can be mainly divided into three types: V_2O_5 with carbonaceous materials, V_2O_5 with conductive polymers, and V_2O_5 with metal oxides.

Carbonaceous materials are considered as good electronic conductors, which also display excellent chemical and electrochemical stability. Therefore, carbon coating is an efficient approach to improve the electrical conductivity as well as chemical and electrochemical stability. Moreover, the good Li^+ ion penetration of carbonaceous materials ensures that carbon coating layer would not impede the contact between Li^+ ion and V_2O_5 [72]. Compositing V_2O_5 with other conductive carbon materials, such as graphene [82] and CNTs [84] or conductive polymers, such as poly(3,4-ethylenedioxythiophene) [95] and polypyrrole [96], can also improve the electrochemical performance.

Considering the poor cycling stability of V_2O_5 in the large potential window (two or three Li^+ ion intercalation/deintercalation per formula for high capacity), some metal oxides with excellent electrochemical stability and mechanical strength, such as TiO_2 [91] and SiO_2 [93], have been utilized to coat V_2O_5 and enhance the cycling stability. For example, the amorphous SiO_2-coated V_2O_5 nanoflake (V_2O_5@SiO_2) arrays were demonstrated to maintain a high capacity of 280 mAh g^{-1} after 100 cycles, which is much higher than that of pure V_2O_5 arrays (149 mAh g^{-1}) [93]. The SiO_2 coating layer plays an important role in the improvement of cycling stability, which restrains the outward swell of internal V_2O_5; meanwhile, the porous structure of SiO_2 coating layer ensures the sufficient contact between V_2O_5 and electrolyte. However, SiO_2 is inactive and do not provide capacity in the high voltage, which will result in sacrifice in capacity of the whole electrode. To improve the cycling stability without sacrifice the capacity at wide voltage window, Niu et al. [89] designed 3D V_2O_5/NaV_6O_{15} hierarchical heterostructures and demonstrated the synergistic effect between V_2O_5 and NaV_6O_{15}. First, the NaV_6O_{15} nanospindles effectively reduce the potential barrier for Li^+ ion intercalation/deintercalation and increase the ionic conductivity. Second, the constant crystal structure of NaV_6O_{15} and the good lattice matching between V_2O_5 and NaV_6O_{15} can greatly reduce the stress caused by Li^+ ion intercalation/deintercalation. Third, V_2O_5 nanosheets backbone is beneficial for increasing the capacity of the hierarchical heterostructures, restraining the self-agglomeration of NaV_6O_{15} nanospindles and maintaining the stability.

3.1.3. Cation-doped V_2O_5

Doping strategy could greatly influence the crystal structure and electronic state of the materials, thereby resulting in the enhancement of electrochemical performance. To overcome the poor electronic conductivity and structural degradation issue of V_2O_5, various elements doping, such as Al [99,110,111], Cr [112], Mn

[98,113], Fe [114], Sn [115], Cu [103], and Ni [101], have been reported to improve the electrochemical performance of V_2O_5. The main distinct advantages of cation-doped V_2O_5 are as follows: (a) cation doping may result in the valence reduction from V^{5+} to V^{4+} or V^{3+}, which could enhance the electronic conductivity; (b) the introduction of metal cations into V_2O_5 may result in the formation of [MO_6] octahedral units, which can improve the stability of the V-O layered structure during the Li^+ ion intercalation/deintercalation, thereby enhancing the cycling stability; (c) the structural defects in metal cation-doped V_2O_5 may provide more Li^+ ion diffusion channel and act as nucleation centers for phase transition during Li^+ insertion/extraction, which also enhances the cycling stability.

When the heteroatoms is doped into V_2O_5 layer, the enhanced electrochemical performance mainly attributed to the formation of low valence vanadium (V^{4+} or V^{3+}) and oxygen vacancies. Song et al. reported the V^{4+} self-doped V_2O_5 (V-V_2O_5) without heteroatoms [102]. The R_{ct} of V-V_2O_5 is much lower than non-doped V_2O_5 (72.8 Ω vs. 263.5 Ω) and the Li^+ ion diffusion coefficient of V-V_2O_5 is about two orders of magnitude higher than that of non-doped V_2O_5. Consequently, the V-V_2O_5 cathode achieves superior cycling stability and rate performance with lower potential polarization.

In summary, as a typical layered cathode material, orthorhombic V_2O_5 has received great attentions in LIBs because of its ability to realize multi-electron reaction for high capacity. However, the contradiction between high capacity and good cycling performance is one of the main challenges toward the practical application of V_2O_5. The investigations about how to improve the cycling stability of V_2O_5 in the case of multilithium intercalation have lasted for decades. Some significant progresses have been achieved with both high capacity and good cycling stability realized. But considering the relatively low voltage, together with the present developing tendency of the dominating LIB cathodes, we believe that the opportunity of V_2O_5 cathode mainly locates at some special energy storage fields in the future, such as flexible electronic devices. Compared with other cathode materials, V_2O_5 with flexible morphology such as ultralong nanowires can be simply synthesized and then the flexible freestanding electrode can be easily fabricated.

3.2. VO_2(B)

Different from orthorhombic V_2O_5, VO_2(B) shows an another kind of layered structure, with [VO_6] octahedron bilayers connected by corner sharing, thus providing a 1D channel for Li diffusion (Fig. 5a) [13,116,117]. The different structure results in different electrochemical properties. VO_2(B) only shows a pair of redox peaks at about 2.5 V both in the potential range of 2–3 V or 1.5–4 V (vs. Li^+/Li) (Fig. 5b). However, the achieved specific capacity is highly relevant to the applied potential range (Table 3). The much higher capacities over 400 mAh g^{-1} were obtained in 1.5–4 V, compared with ~200 mAh g^{-1} in 2–3 V (Fig. 5c and d). But the origin of the big difference in capacity at different potential range is still ambiguous. It requires a deeper insight about the detailed Li^+ storage mechanism and structure evolution of VO_2(B). Even so, the high capacity of VO_2(B) makes it a promising LIB cathode. Moreover, the share corner connection between bilayers enhances the structural stability of VO_2(B), which is beneficial for the cycling stability of LIBs. Recently, various nanostructured VO_2(B) and VO_2(B)-based composites have been fabricated to optimize the electrochemical performance as cathode materials for LIBs (Table 3).

The mesoporous VO_2(B) nanowires with diameter of about 80–100 nm have been obtained from the decomposition of $NH_4V_3O_8$ nanowires [119], which exhibits a capacity retention of 90% after 500 cycles. Assembling the 1D nanowire into hierarchical structure is an effective approach to overcome the self-aggregation of the nanowires and increase the electrochemical reaction kinetics. Niu et al. [120] reported the VO_2(B) nanowires-assembled hollow hierarchical microspheres. At the voltage range of 2–3 V, VO_2(B) hollow microspheres cathode exhibits a high capacity over 200 mAh g^{-1} at 100 mA g^{-1} and remains at 134 mAh g^{-1} at 2000 mA g^{-1}, which is much higher than that of VO_2(B) nanowires (46 mAh g^{-1}). Moreover, the VO_2(B) hollow microspheres exhibit enhanced cycling stability with capacity retention of 73% after 1000 cycles. The nanoscroll-buffered hybrid nanostructural VO_2(B) (HNS) was designed and synthesized by Mai et al. [121], which exhibits enhanced cycling stability (retained over 82% after 1000 cycles) and rate capability. The as-synthesized HNS is composed of nanowires, nanobelts, and nanoscrolls, and the nanoscrolls act as a buffered section to accommodate the volume expansion/shrinkage during the intercalation/deintercalation of Li^+ ions, enhancing the cycling stability of HNS.

Nanostructures enhance the electrochemical performance of VO_2(B), but the improvement is limited in some aspect, especially the electronic conduction. To further improve the electrochemical performance of VO_2(B), carbon materials have been introduced to form VO_2(B)/carbon materials nanocomposites. The carbon-coated VO_2(B) nanobelts (VO_2(B)@C) with different carbon content (4.2 wt %, 6.6 wt%, 8.4 wt%, and 9.6 wt%) were obtained by Rui et al. [123]. As cathode materials for LIBs, the VO_2(B)@C with 6.6 wt% carbon (VO_2(B)@C (6.6 wt%)) displays best cycling stability and rate performance. Based on the electrochemical analysis, VO_2(B)@C (6.6 wt %) displays the lowest charge-transfer resistance among the four samples, whereas the lithium-ion diffusion coefficient of VO_2(B)@C reduces with the increase of carbon content. It indicates that the lower carbon content will result in low electronic conductivity, while the higher carbon content will reduce the mass ratio of active materials and hinder the diffusion of Li^+ ion. Except for amorphous carbon, some carbon nanomaterials including CNTs [124,132] and graphene [125–127,133,134] also have been utilized to improve the electrochemical performance of VO_2(B). For example, Yang et al. [126] synthesized the VO_2(B)/graphene nanoribbons (VO_2-graphene) via hydrothermal method (Fig. 6a and b). The VO_2-graphene cathode (the content of VO_2 is 78%) exhibits a reversible capacity of as high as 415 mAh g^{-1} in 1.5–3.5 V (Fig. 6c). Even at the high rate of 190 C, the capacity still remains at 204 mAh g^{-1} with the capacity retention of over 90% after 1000 cycles.

Besides, the conductive substrates, such as graphene foam (GF) [135], carbon fiber cloth [131], and Ni foam [128] have been used to fabricate the binder-free VO_2(B)-based nanocomposites cathode. Chao et al. designed a binder-free graphene quantum dots (GQDs)–coated VO_2 biface arrays using GF as the substrate (Fig. 6d and e) [129]. The VO_2 nanobelt shows a thickness of about 15 nm, and the GQDs layer is about 2 nm in thickness. The GF and GQDs together with the nanobelt arrays provide fast and short electron/ion transport pathways, resulting in outstanding rate performance. Meanwhile, the integrated structure effectively avoids the 'dead' mass, and the inner space and high surface area facilitate the electrolyte-active material contact, ensuring the utilization of active materials and high capacity. When cycled in the voltage range of 1.5–3.5 V, a high capacity of more than 420 mAh g^{-1} at 1/3 C was achieved, and excellent cycling stability with capacity retention of 94% after 1500 cycles at 60 C was demonstrated (Fig. 6f).

In brief, VO_2(B) is the other typical high-capacity cathode for lithium batteries. Compared with V_2O_5, the share corner connection property in the crystal structure endows it a better structure stability. Besides, the single redox couple avoids the irreversible phase change observed in the case of V_2O_5 during multilithium intercalation/de-intercalation. These merits make VO_2(B) more promising to realize both high capacity and good cycling stability,

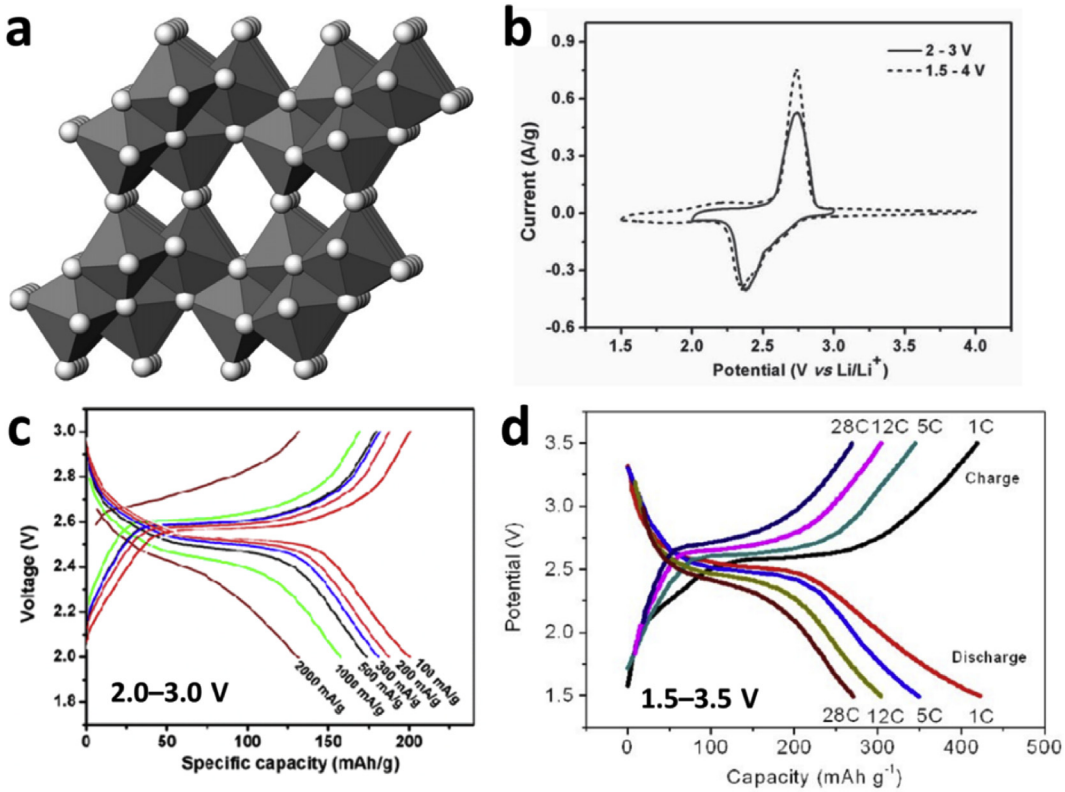

Fig. 5. (a) Crystal structure of VO_2(B). (b) CV curves of VO_2(B) for Li storage at voltage range of 2–3 V and 1.5–4 V (vs. Li^+/Li). (c) Charge/discharge profiles of VO_2(B) for Li storage at different current densities between 2.0 and 3.0 V (vs. Li^+/Li). (d) Charge/discharge profiles of VO_2(B) for Li storage at different current rates between 1.5 and 3.5 V (vs. Li^+/Li). Reproduced with permission from (a) Elsevier [116], (b) Wiley VCH [121], (c) American Chemical Society [120] and (d) American Chemical Society [126]. CV, Cyclic voltammetry.

Table 3
The Li-storage performance of partial VO_2-based cathode materials.

Materials	Potential window (V vs. Li^+/Li)	Maximal capacity (mAh g^{-1}/mA g^{-1})	Cycling performance	Rate performance (mAh g^{-1}/mA g^{-1})	References
VO_2 ultra-thin nanowires	2.0–3.2	265/10	~65% after 50 cycles	–	[116]
Nanothorn VO_2 hollow microsphere	1.5–4.5	450/10	Without fading after 50 cycles	195/50	[118]
Mesoporous VO_2 nanowires	2.0–3.0	188/100	90% after 500 cycles	101/1000	[119]
VO_2 nanowire-assembled hollow microspheres	2.0–3.0	203/100	80% after 1000 cycles	134/2000	[120]
Nanoscroll-buffered hybrid nanostructural VO_2	2.0–3.0	158/100	82% after 1000 cycles	98/2000	[121]
VO_2/C nanobelts	1.5–4.0	220/50	69.8% after 100 cycles	138/1000	[122]
VO_2/C nanobelts	2.0–4.0	161/100	80% after 50 cycles	100/2000	[123]
VO_2 nanowires/CNTs composites	1.5–3.5	~200/95	~94% after 100 cycles	~60/1900	[124]
VO_2 nanotube–graphene hybrid	1.5–4.0	450/40	80% after 20 cycles	200/100	[125]
Single-crystalline VO_2-graphene ribbons	1.5–3.5	415/415	93% after 1000 cycles	204/37200	[126]
N-doped graphene–VO_2 nanosheet-built 3D flower hybrid	1.5–4.0	418/50	60% after 50 cycles	102/5000	[127]
Vertically aligned VO_2/graphene nanobelt forest	1.5–3.5	475/100	79% after 2000 cycles	100/27000	[128]
Graphene quantum dots–coated VO_2 arrays	1.5–3.5	421/100	85% after 1500 cycles	151/36000	[129]
Carbon quantum dot surface–engineered VO_2 interwoven nanowires	1.5–3.5	427/100	112% after 500 cycles	168/19200	[130]
Carbon fiber cloth@VO_2 (B) nanobelt arrays	2.0–3.0	145/100	90% after 200 cycles	91/2000	[131]

as demonstrated by the reported results mentioned above. However, VO_2(B) is a metastable phase in thermodynamics with a low vanadium valence, which determines that the controllable synthesis and mass production is more challenging than that of V_2O_5.

3.3. LiV_3O_8

Since the first report as a LIB cathode by Nassau et al., in 1981 [136], LiV_3O_8 has been paid great attentions in the past decades because of its high capacity, moderate output voltage, and good structural reversibility during lithiation/delithiation. LiV_3O_8 also shows a typical layered structure with $(V_3O_8)^-$ layers pillared by Li^+ ions in the interlayers along *a* axis [13]. When used as a cathode material in LIBs, the Li^+ ions in LiV_3O_8 is immobile in the structure, whereas more than three Li^+ ions can be intercalated per unit. The theoretical capacity is ~279 mAh g^{-1} when three Li^+ inserted and ~373 mAh g^{-1} when four Li^+ inserted [137,138]. There are multiple voltage plateaus in the discharge curve of LiV_3O_8, indicating the

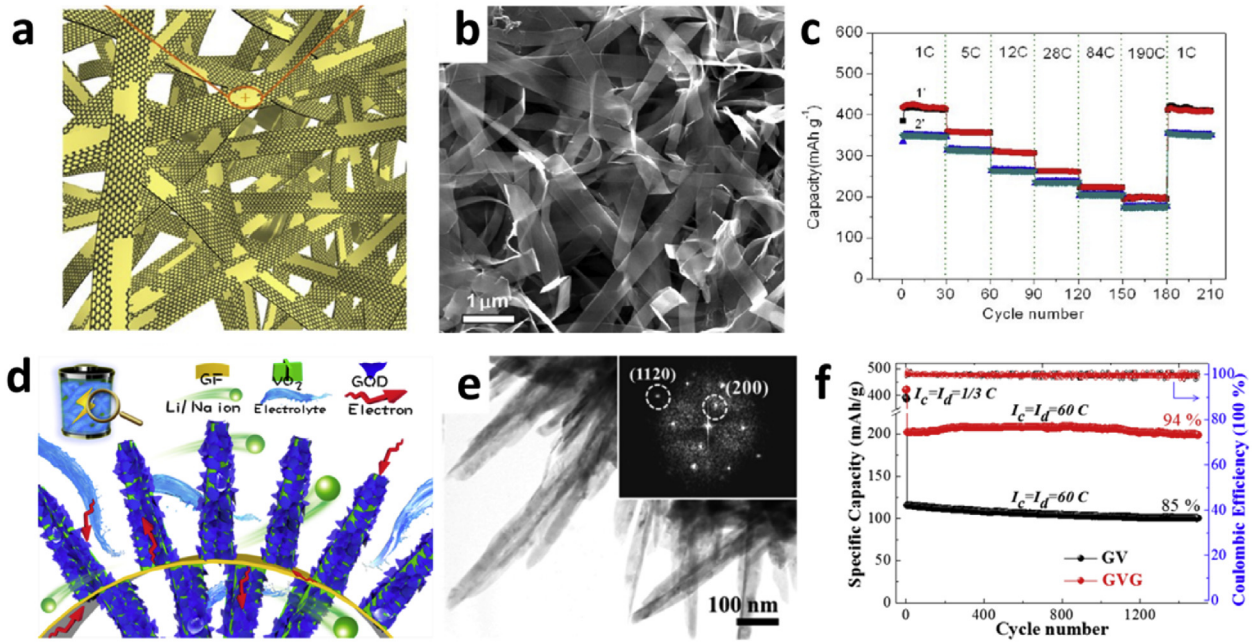

Fig. 6. (a) The illustration of VO_2(B)/graphene nanoribbons. (b) Scanning electron microscopy (SEM) image of VO_2(B)/graphene nanoribbons. (c) Rate capability of VO_2(B)/graphene nanoribbons with different VO_2 content from 1 C to 190 C. (d) The illustration of binder-free graphene quantum dots (GQDs) coated VO_2 biface arrays for fast Li/Na storage. (e) Transmission electron microscopy (TEM) image of VO_2@GQDs arrays; inset is the fast Fourier transform (FFT) pattern. (f) The cycling performance of VO_2@GQDs arrays and VO_2 arrays at 60 C for 1500 cycles. Reproduced with permission from (a–c) Ref. [126] and (d–f) Ref. [129] from American Chemical Society.

multistep insertion of Li^+ ions. The average voltage is about 2.6 V, which together with the theoretical capacity, manifests a high theoretical energy density of 728–967 Wh kg^{-1}.

The main drawback of LiV_3O_8 lies in the low Li^+ diffusion coefficient (~10^{-13} cm^2 s^{-1}) together with poor electronic conductivity (~10^{-6} S cm^{-1}) [138], which results in the unfavorable cycling and rate performance in most cases. The synthesis methods were found to have a distinct effect on the electrochemical performance in previous studies [139–141], which can be explained by the fact that different synthesis methods have different impacts on the degree of crystallinity, particle size, surface state and defects, and then affect the electronic conductivity and Li^+ diffusion coefficient. To improve the electrochemical performance of LiV_3O_8 as LIB cathode, lots of strategies have been proposed in the past years, including nanostructure design [137,142–144], surface modification [145–149], conductive coating [150–155], metal ions doping [145,156] and oxygen-deficient introduction [138], *etc.*

Decreasing the particle size to nanoscale will certainly shorten the Li^+ diffusion distance and then improve the charge/discharge kinetics. The first nanoscale LiV_3O_8 was reported by Xu et al., in 2004 [157]. The LiV_3O_8 nanorods were prepared based on the hydrothermal reaction, and it exhibited a highest discharge capacity of 302 mAh g^{-1} in the voltage range of 1.8–4.0 V. After 30 cycles, a capacity of 278 mAh g^{-1} can be remained. Pan et al. [143] fabricated nanosheet-structured LiV_3O_8. The calcined sample at 500 °C delivers a high discharge capacity over 260 mAh g^{-1} at 100 mA g^{-1}, with no capacity fading after 100 cycles. To further improve the high rate and long-term cycling performance, Xu et al. fabricated ultralong LiV_3O_8 nanowires with large aspect ratios using a topotactical synthesis method [144]. The $H_2V_3O_8$ nanowires were selected as the precursor because it has a similar layered structure with LiV_3O_8 (Fig. 7a). The obtained LiV_3O_8 nanowires by topotactic Li intercalation maintained the ultralong morphology of $H_2V_3O_8$ nanowires. When used as a LIB cathode, high capacities over 300 mAh g^{-1} were obtained at 20 mA g^{-1} (Fig. 7b) with good cycling stability. Besides, the LiV_3O_8 nanowires showed superior high-rate performance with discharge capacity of 137 mAh g^{-1} at a high current density of 2000 mA g^{-1}. Even after 600 cycles, a capacity of 120 mAh g^{-1} was maintained, corresponding to a capacity retention of 87.6%.

On the basis of the nanostructure design, the performance of LiV_3O_8 can be further improved by surface modification, conductive decoration or metal ions doping. For example, Al_2O_3-modified LiV_3O_8 were demonstrated to exhibit improved cycling stability, which may be because of the protective effect of Al_2O_3 layer to prevent the potential side-reaction of the nanosized electrode [146–148]. Another facile surface modification strategy was reported by Sun et al., which involved a self-transformation of superficial LiV_3O_8 to $Li_xV_2O_5$ under the H_2-reduction atmosphere [149]. The $Li_xV_2O_5$ layer can be well controlled with different thickness, and the combination between $Li_xV_2O_5$ and LiV_3O_8 was thought to be more compact than other coating strategies (Fig. 7c). Besides, the $Li_xV_2O_5$ has a much higher Li^+ diffusion coefficient than LiV_3O_8. As a result, the $Li_xV_2O_5/LiV_3O_8$ nanoflakes showed enhanced cycling stability (82% retention after 420 cycles at 1 C) and much improved rate capability (Fig. 7d and e). Conductive decoration such as carbon coating is another way that was widely used to address the issue of low electronic conductivity. However, the carbon-coated LiV_3O_8 has rarely been reported, which may be attributed to that vanadium exists as V^{5+} in LiV_3O_8, whereas carbon coating is always achieved at the condition of reduction atmosphere. But graphene decorated LiV_3O_8 nanocomposites have been reported by many groups, such as LiV_3O_8/rGO ultradispersed nanoarchitecture [151], graphene nanosheet–wrapped LiV_3O_8 nanocomposites [152] and sandwich-like LiV_3O_8/graphene multilayer nanomembranes [153], *etc.* These nanocomposites displayed improved cycling and rate performance because of the greatly enhanced electron/ion transport. Some other conductive decorated nanocomposites such as LiV_3O_8/PANI [154], LiV_3O_8/Ag [158] and Cr-coated LiV_3O_8 [155] were also reported. Metal ions doping is also an

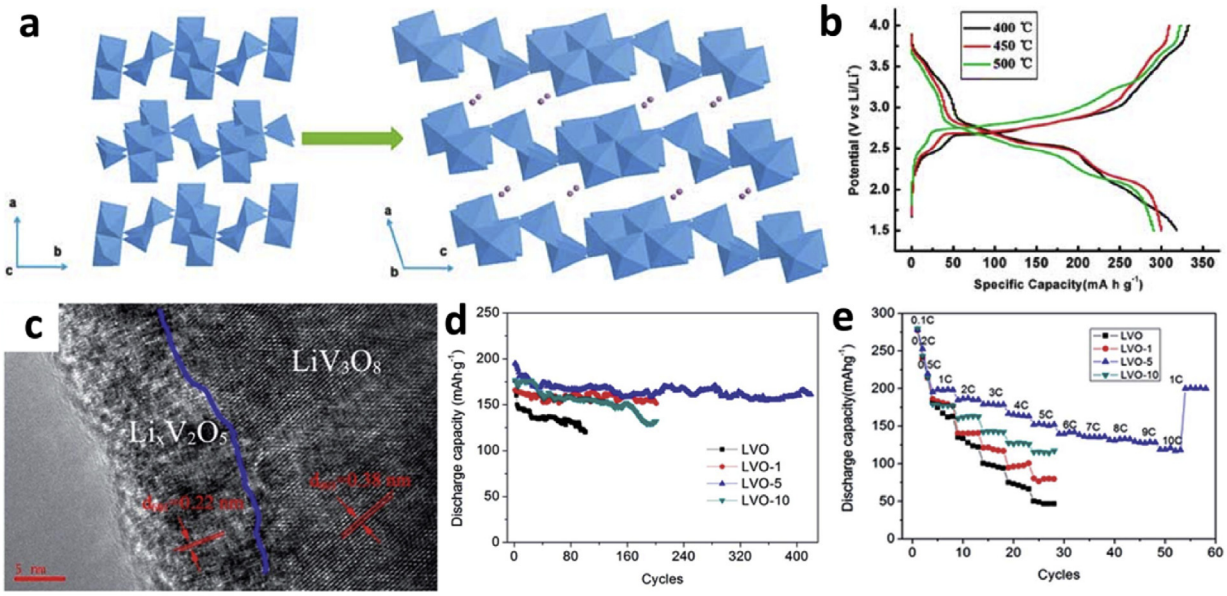

Fig. 7. (a) The illustration of crystal structure transformation from $H_2V_3O_8$ to LiV_3O_8. (b) The charge-discharge profiles of ultralong LiV_3O_8 nanowires at current density of 20 mA g^{-1}. (c) The high-resolution TEM image of $Li_xV_2O_5/LiV_3O_8$ nanoflakes. (d,e) Cycling stability (d) and rate capability (e) of bare LiV_3O_8 and $Li_xV_2O_5/LiV_3O_8$. Reproduced with permission from (a–b) Nature Publishing Group [144] and (c–e) The Royal Society of Chemistry [149].

effective approach to increase the electronic conductivity and ion diffusion coefficient. Song et al. [156] reported Mo-doped LiV_3O_8 nanorods, in which 25% V^{4+} and 3.5% oxygen vacancies were demonstrated by X-ray photoelectron spectroscopy measurements. The reduced valence state of vanadium and introduced oxygen vacancies resulted in an increased electronic conductivity and a more open structure for Li^+ diffusion, which lead to the increased electrochemical reversibility, reduced reaction resistance, and enhanced Li^+ diffusivity.

When it comes to the practical application of LiV_3O_8, there is another important aspect that has to be discussed. Different from the commercialized LIB cathodes, such as $LiCoO_2$ and $LiFePO_4$, the Li ions in the crystal structure of LiV_3O_8 is immobile, which determine that LiV_3O_8 cannot match with commercial graphite anode but has to match with the Li-rich anode (mainly metallic Li anode) for applications, the same case with V_2O_5 and VO_2. However, using metallic Li as anode still suffer from dendrite growth and safety issues, which seriously hinders the practical application of LiV_3O_8 and other non-lithiated cathodes [28,155]. But it is comforting that the lithium-rechargeable batteries using Li-metal anodes have regained attentions recently, and the investigations about Li-metal anodes have achieved significant progresses [159,160]. Considering the high capacity and moderate voltage, a high theoretical energy density of 728–967 Wh kg^{-1} can be obtained for LiV_3O_8, which means an energy density of 250–350 Wh kg^{-1} can be expected for the LiV_3O_8//Li full batteries, much higher than the value achieved for the present commercial LIBs (130–180 Wh kg^{-1}). As the progress of Li metal anodes in the future, rechargeable lithium batteries will be promising to act as the next-generation battery technology for high power and high energy density, and LiV_3O_8 is expected to be one of the choices for the cathodes.

3.4. $VOPO_4$ and $LiVOPO_4$

Different from the abovementioned vanadium oxides or lithium vanadium oxide, $VOPO_4$ belongs to vanadyl phosphate, which is constructed by [VO_6] octahedrons and [PO_4] tetrahedron (Fig. 8a). Ascribe to the existence of [PO_4] group, $VOPO_4$ exhibits higher work potential than vanadium oxides when used as lithium battery cathodes. $VOPO_4$ has many polymorphs. The reported phases include α_I (*P*4/n), α_{II} (*P*4/n), β (*P*nma), δ ($P4_2$/mbc), ε (*C*c), ω ($P4_2$/mmc), and γ (*P*bam) [161,162]. Such a complex phase variation makes it a challenge to synthesize a specific pure phase and study the structure-performance relationships. This may explain why the investigations about $VOPO_4$ for energy storage mainly centered in recent years. In 2003, Azmi et al. [161] systematically synthesized all these seven phases and compared their electrochemical properties. They found that the Li^+ intercalation capacity is highly dependent on the crystal structure. Among these different phases, ε-$VOPO_4$ (Fig. 8a) attracted much attention for high-energy lithium battery cathode recently, because of its multi-electron reaction property. It has been demonstrated that ε-$VOPO_4$ can realize two Li^+ intercalation/deintercalation, whereas very few other phosphate cathodes can realize more than one Li^+ insertion per transition metal ions. One Li^+ insertion into ε-$VOPO_4$ corresponds to a theoretical capacity of 166 mAh g^{-1} with a high potential of ~4.0 V (V^{5+}/V^{4+} redox couple), which suggests that a higher energy density of $VOPO_4$ than $LiFePO_4$ can be achieved [163]. If two Li^+ are intercalated, the theoretical capacity would increase to over 300 mAh g^{-1} with an additional voltage plateau at ~2.5 V (V^{4+}/V^{3+} redox couple) (Fig. 8b), which results in a high specific energy density of the cathode over 900 Wh kg^{-1} [164]. Such a high energy density is very attractive; however, poor kinetics and fast capacity fading are major obstacles in the way to realize two Li^+ reaction.

In recent years, Whittingham group carried out extensive studies about the two Li^+ reaction of ε-$VOPO_4$ for LIBs [162,164–168]. They found that the first Li^+ insertion (4.5–3.0 V vs. Li^+/Li) is a single two-phase reaction from ε-$VOPO_4$ to ε-$LiVOPO_4$ (Fig. 8c), while two intermediate phases of $Li_{1.5}VOPO_4$ and $Li_{1.75}VOPO_4$ was observed during the second Li^+ intercalation (3.0–1.5 V vs. Li^+/Li), reflected by the additional two voltage plateaus in the low voltage (Fig. 8e). Besides, it was found that the first Li^+ intercalation shows a much lower kinetics than that of the second Li^+ (Fig. 8d and f) [164]. The deep investigations indicate that the capacity fading in the case of two Li^+ intercalation is ascribed to the disrupted kinetics in the high voltage regime, which

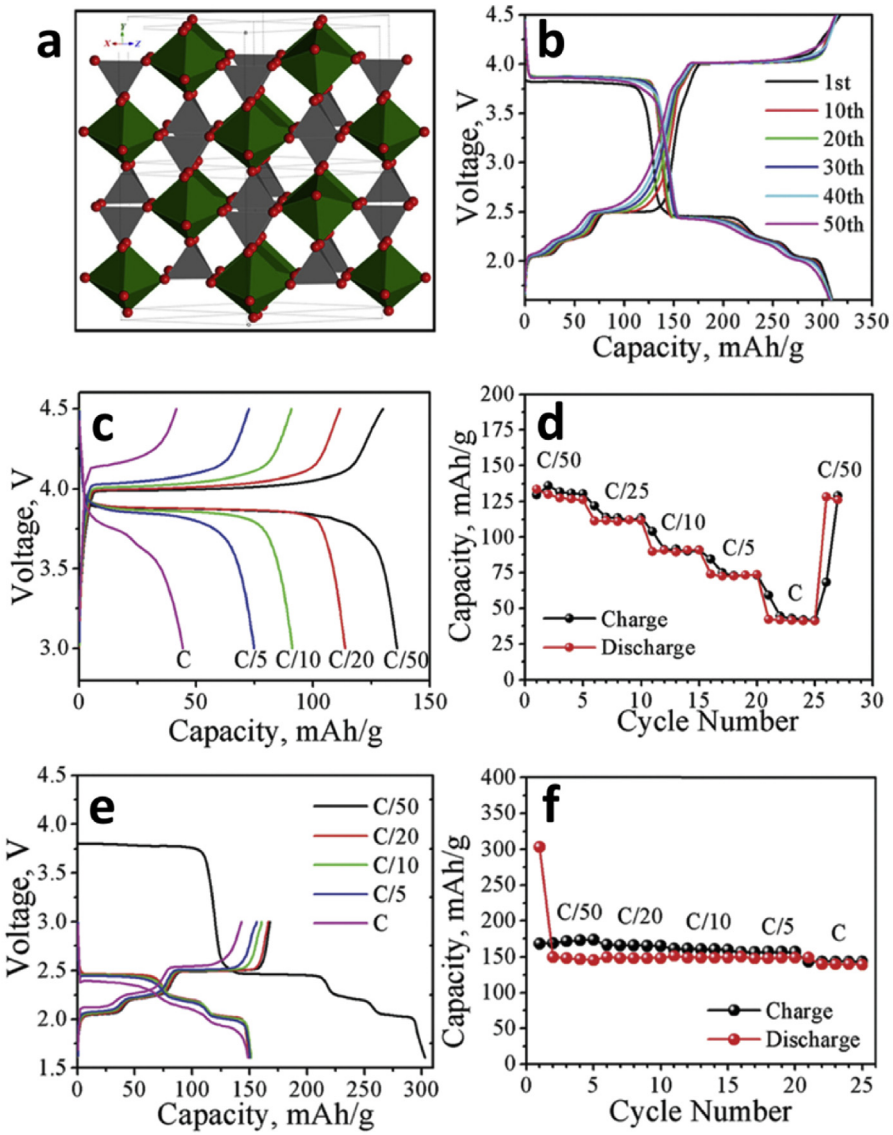

Fig. 8. (a) Crystal structure of ε-$VOPO_4$; the green polyhedrons represent [VO_6] octahedrons, grey polyhedrons represent [PO_4] tetrahedron, and red balls represent oxygen atoms. (b) Charge/discharge profiles of ε-$VOPO_4$ in the potential range of 1.6–4.5 V (vs. Li^+/Li) at C/50. (c,d) Charge/discharge profiles (c) and rate performance (d) of ε-$VOPO_4$ in the potential range of 3.0–4.5 V (vs. Li^+/Li). (e,f) Charge/discharge profiles (e) and rate performance (f) of ε-$VOPO_4$ in the potential range of 1.6–3.0 V (vs. Li^+/Li). Reproduced with permission from (a) Elsevier [166] and (b–f) The Royal Society of Chemistry [164].

hinder the full two Li^+ capacity [169]. Based on the electrochemical tests and density functional theory calculations, it is shown that Li_xVOPO_4 is likely to be a pseudo-1D ionic conductor (lithium diffusion coefficient: 10^{-10} to 10^{-9} cm^2 s^{-1}) with low electronic conductivity, which suggests that nanosizing and carbon coating is necessary to realize good electrochemical performance [170].

Nanostructured ε-$VOPO_4$ with a diameter of 150 nm was demonstrated to exhibit a reversible capacity of 180 mAh g^{-1}, after an initial capacity of 227 mAh g^{-1} in the voltage range of 2.0–4.3 V. After 110 cycles, a capacity of 165 mAh g^{-1} was retained [165]. The β-$VOPO_4$/ε-$VOPO_4$ composite with irregular shaped particles of appropriately 100–400 nm in diameter was also synthesized, which was found to exhibit improved cycling stability in the potential range of 2.0–4.3 V. A high initial capacity of 207 mAh g^{-1} at 0.082 mA cm^{-2} (C/7.5) was achieved. Good cycling stability with retention of 88% (relative to the capacity of the second cycle) after 200 cycles at 0.164 mA cm^{-2} was demonstrated [166]. Mo substitution is the other strategy to enhance the electrochemical performance of ε-$VOPO_4$ in the wide voltage range of 2.0–4.5 V. A high reversible capacity of 250 mAh g^{-1} (~1.6 Li) in the initial cycle at C/25 was obtained, which retained about 200 mAh g^{-1} after 20 cycles. The faster kinetics and lower voltage hysteresis were demonstrated for the Mo-substituted sample [168]. Even though these optimizing strategies improved the cycling stability of ε-$VOPO_4$, the full capacity of two Li^+ reaction is still not released. Recently, Whittingham group further synthesized uniform shaped cubic ε-$VOPO_4$ with primary particles of ~100–200 nm [164]. To increase the electronic conductivity, 15 wt% graphene nanoplatelets was hand milled with the sample. It was found that the graphene nanoplatelets form a conductive network between the particles, which would effectively increase the electronic and ionic conductivity. When cycled in the voltage range of 1.6–4.5 V at C/50, a high discharge capacity of 305 mAh g^{-1} with good stability for 50 cycles was displayed. The obtained capacity basically reached the

theoretical value of 2 Li^+ intercalation, further demonstrating the important role of nanosizing and conductive decoration for the full release of the capacity.

Note that $VOPO_4$ is a Li-poor cathode, which can be only matched with lithiated anodes or metallic lithium anode. Recently, $LiVOPO_4$, which is the lithiated member of $VOPO_4$, was found to be obtained through chemical synthesis methods [171] or even solid-state reaction approach [170]. There are three different polymorphs of $LiVOPO_4$, namely ε-$LiVOPO_4$ (triclinic), β-$LiVOPO_4$ (orthorhombic), and α_I-$LiVOPO_4$ (tetragonal) [172]. Among them, layered α_I-$LiVOPO_4$ was demonstrated to be a metastable phase, which was less studied due to its instability in thermodynamics [173]. Manthiram et al. reported that a high reversible capacity of 225 mAh g^{-1} (1.4 Li^+ reaction) at C/20 can be achieved for this metastable phase [174]. For ε-$LiVOPO_4$ and β-$LiVOPO_4$, Whittingham et al. recently systemically compared their thermodynamics stability and electrochemical performance. It was shown that ε and β phases have little difference in Gibbs free energy. With $LiVOPO_4 \cdot 2H_2O$ as the same precursor, it was found that β-$LiVOPO_4$ can be easily achieved in the oxygen-rich atmospheres while ε-$LiVOPO_4$ was obtained in Ar atmospheres after high temperature annealing (Fig. 9a). The electrochemical performance shows that β-$LiVOPO_4$ shows a better rate capability than ε phase, which was proposed because of the increased presence of facets with superior ion diffusion at the surface of β-$LiVOPO_4$ [173].

Achieving high electrochemical performance in the case of two Li^+ reaction is the ultimate target for the application of $LiVOPO_4$. Very recently, an impressive performance of ε-$LiVOPO_4$ was reported by Whittingham and coauthors [175]. ε-$LiVOPO_4$/C was synthesized by a facile solid state method and ball-milling approach. To remove the disorder in the ball-milled process, which was demonstrated to be harmful to the performance [176,177], a postannealing of the ball-milled composite at 450 °C in Ar atmosphere was applied (Fig. 9b). The finally obtained ε-$LiVOPO_4$ with reduced disorder shows a high capacity of 270 mAh g^{-1} at C/5. The good stability for 100 cycles with capacity fading less than 4% was demonstrated, which was much better than that of the disordered ε-$LiVOPO_4$ (Fig. 9c–e).

3.5. $Li_3V_2(PO_4)_3$

$Li_3V_2(PO_4)_3$ (LVP) is an another important and promising phosphate cathode with multi-electron reaction property, which has recently attracted extensive attentions as LIB cathode because of its high theoretical capacity, high thermal stability, and high working potentials [18,178–180]. LVP has two different crystal frameworks (monoclinic phase and rhombohedral phase) based on the different connectivity between $[PO_4]$ tetrahedra and $[VO_6]$ octahedral [18,181,182]. Most of the studies focused on the monoclinic LVP because the rhombohedral phase (NASICON structure) can only be achieved by ion exchange from NASICON $Na_3V_2(PO_4)_3$ [183]. The monoclinic LVP delivers a 3D open framework (Fig. 10a) with high thermodynamic stability. The 3D open framework consists of slightly distorted $[VO_6]$ octahedra and $[PO_4]$ tetrahedra which are linked together by sharing oxygen atoms to form a $(M–O–P–O)_n$ bonding arrangement [184]. Clearly, there are three distinct lithium atoms occupying three different crystallographic positions in the structure (Fig. 10a). It has been demonstrated that the monoclinic LVP has a fast Li^+ diffusion coefficient ranging from 10^{-9}–10^{-10} cm^2 s^{-1}, which is about five orders of magnitude higher than that of commercialized $LiFePO_4$ (10^{-14}–10^{-16} cm^2 s^{-1}) [18,182]. Besides, up to three Li^+ can be extracted from LVP [18,182,185], corresponding to a high theoretical capacity of 197 mAh g^{-1} (Fig. 10b).

When cycled in the voltage range of 3.0–4.4 V (vs. Li^+/Li), reversible insertion/extraction of two Li^+ can be realized for LVP, with three discharge plateaus at about 3.58, 3.66, and 4.05 V (Fig. 10c). To realize three Li^+ transportation, the upper limit of the voltage has to be expanded to 4.8 V. However, in such case, LVP exhibits different charge/discharge plateaus during delithiation/

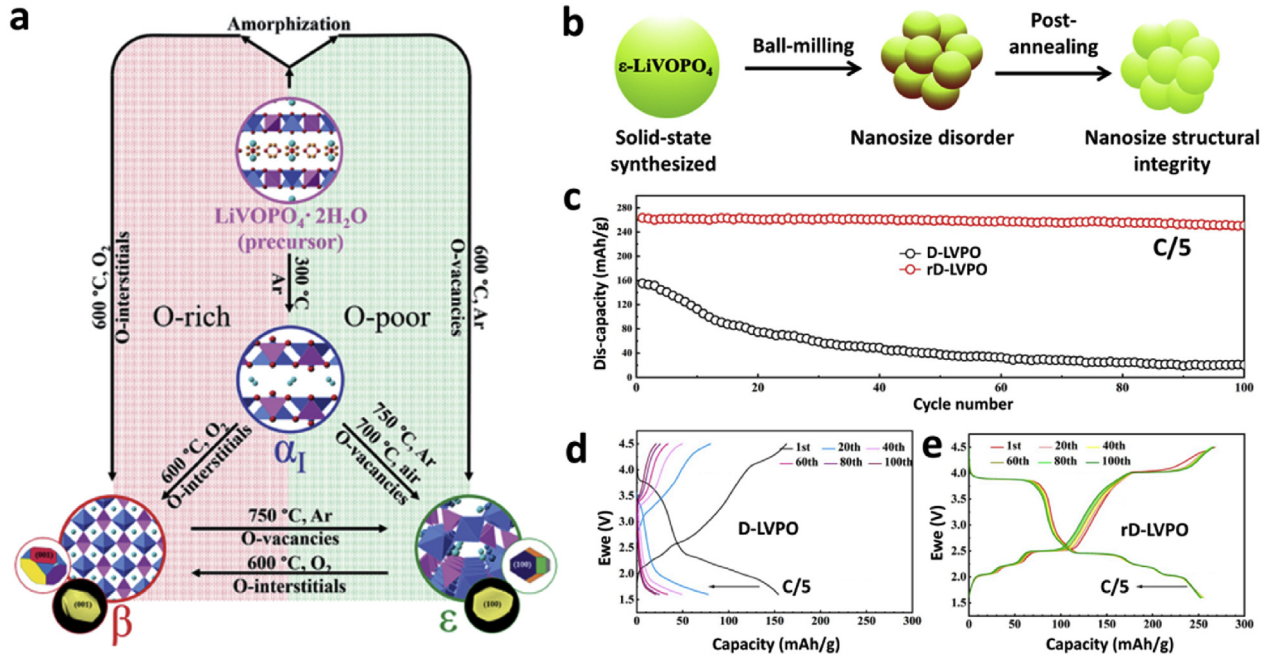

Fig. 9. (a) Illustration of the transformation condition of β-$LiVOPO_4$ and ε-$LiVOPO_4$. (b) Illustration of the process of disorder removed nanosized ε-$LiVOPO_4$. (c) Comparison of the cycling stability of disordered ε-$LiVOPO_4$ and disorder removed ε-$LiVOPO_4$ at C/5. (d,e) Charge/discharge profiles of disordered ε-$LiVOPO_4$ (d) and disorder removed ε-$LiVOPO_4$ (e) in the potential range of 1.6–4.5 V (vs. Li^+/Li) at C/5. Reproduced with permission from (a) The Royal Society of Chemistry [173] and (b–e) Elsevier [175].

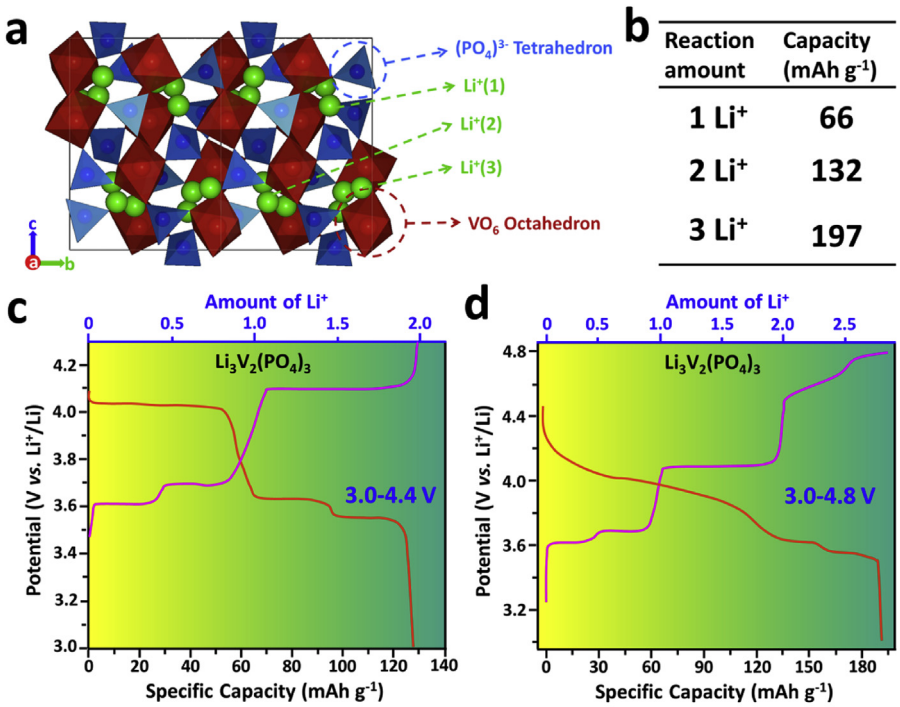

Fig. 10. (a) Crystal structure of LVP along *a*-axis. (b) The reaction amount of Li^+ and the corresponding specific capacities. (c,d) Charge/discharge curves and corresponding Li^+ insertion/extraction amounts of LVP at 3.0–4.4 V and 3.0–4.8 V, respectively. LVP, $Li_3V_2(PO_4)_3$.

lithiation, especially in the discharge process (Fig. 10d). It is believed that the observed sloping plateau is resulted by the solid solution behavior (single-phase reaction) during the Li^+ reinsertion into $V_2(PO_4)_3$, because the mixed V^{4+}/V^{5+} state in $V_2(PO_4)_3$ does not display charge ordering, therefore resulting in a disorder of Li^+ reinsertion [182,185].

It has been demonstrated that the cycling performance in the case of three Li^+ reaction is much poorer than that of two Li^+ reaction [186–192]. Ascribe to that, most of the previous works of LVP focused on the electrochemical properties in the case of two Li^+ reaction. Like many other phosphate cathodes, low electrical conductivity of LVP (2.4×10^{-7} S cm^{-1}) [18] is one of the main drawbacks that affects its performance. To increase the electrical conductivity and enhance the electrochemical performance of LVP, a large amount of research works have been carried out using different strategies, including carbon coating combined with nanostructure design, metal ions doping, and multicomponent synergies. Combining carbon coating with nanostructures is a popular optimizing strategy for LVP, which can both increase the electric conductivity and ion diffusion kinetics. Because of the low valence state of vanadium (V^{3+}) and high thermodynamic stability of LVP, it is easy to fabricate carbon-coated LVP with pure phase and high crystallinity at reduction or inert atmosphere. Therefore, with improved electronic conductivity and increased ion diffusion kinetics, together with excellent structure stability in the case of two Li^+ reaction, considerable superior electrochemical performances of nanostructured LVP/C as LIB cathode have been reported. For example, 1D mesoporous LVP/C nanotubes was demonstrated to exhibit ultrastable cycling performance for 9500 cycles [193]. LVP 3D foams was reported to exhibit ultrafast rate capability with no obvious capacity fading over 1000 cycles at a high rate of 100 C [194]. These detailed progresses have been reviewed by Rui et al. [182] and Liu et al. [18] recently.

However, in the case of two Li^+ reaction, the theoretical capacity is only 132 mAh g^{-1}, with specific energy of ~520 Wh kg^{-1}, which shows no obvious advantage compared with the commercialized cathodes. Besides, the other important factor also needs a further attention, which is the low density of LVP (as shown in Table 1). The theoretical density of $LiCoO_2$, $LiMn_2O_4$, and $LiFePO_4$ are about 5.06, 4.23, and 3.62 g cm^{-3}, respectively, while that for LVP is only about 2.88 g cm^{-3}. The low theoretical density of LVP means low tap/compact density and thus low volumetric energy density. Considering the low density feature of LVP (low volumetric energy density), combined with the present obtained superior electrochemical performance of LVP in the case of two Li^+ reaction, it is expected that being used in stationary batteries for large-scale energy storage where allow batteries with a large size will be an important application direction for LVP. Besides, LVP may be also a good choice for batteries used in special conditions. For one thing, when charged at a high frequency large current produced by triboelectric nanogenerator, it is demonstrated that LVP/C nanocomposites showed the best pulse power storage (with a high energy conversion efficiency of 83.4%) compared with $LiFePO_4$, $LiCoO_2$, and $LiMn_2O_4$ [195]. For another thing, because of the high Li^+ diffusion coefficient and excellent thermodynamic stability of LVP, the carbon-coated LVP nanostructures with increased electronic conductivity and enhanced interfacial stability are potential to enable superior electrochemical performance at both low and high temperatures for practical application. For example, the synthesized carbon-coated LVP/C cathode by Qiao et al. [196] shows an outstanding low-temperature and high-temperature performance with high initial discharge capacities of 84.3, 111.1, 128.7, 129.2, and 132.1 mAh g^{-1} at −20, 0, 25, 40, and 65 °C, respectively.

To ensure the sufficient energy density, extending the upper voltage limit to 4.8 V for three Li^+ reaction seems to be necessary for LVP. However, considerable works have manifested that the

cycling stability and rate capability in 3.0–4.8 V are inferior to that in 3.0–4.3 V. Therefore, how to improve the electrochemical properties of LVP in the case of three Li^+ reaction is very important. Recently, Cui et al. [197] reported LVP/C cathode decorated with nitrogen-doped graphene sheets. The hybrid nanocomposites exhibit a high specific discharge capacity of 191.5 mAh g^{-1} at 0.1 C within the voltage range of 3.0–4.8 V (Fig. 11a). Besides, an excellent cycling stability for 1000 cycles at 20 C with only 12.7% capacity loss was also demonstrated at the wide voltage range (Fig. 11b). Full cells using the as-prepared LVP/C as cathode and graphite as anode were also assembled (Fig. 11c), and a high energy density of 136 Wh kg^{-1} was obtained with good cycling stability for 500 cycles (Fig. 11d), which is higher than that based on $LiFePO_4$ cathode (~120 Wh kg^{-1}). This work demonstrates that LVP cathodes can also realize superior performance at the wide voltage range of 3.0–4.8 V with high capacity and high output voltage.

Further optimizing the electrochemical properties of LVP in the case of three Li^+ reaction in the voltage range of 3.0–4.8 V is a very important direction in the future. Besides, deeper insights about the detailed structure evolution and degradation mechanism are required. As the problem of capacity fading under high voltage is solved by potential strategies, the high capacity and high voltage of LVP will be exerted, and then the application of LVP electrode will be further expanded.

4. Vanadium-based multi-electron reaction anodes

Apart from cathodes, some vanadium-based materials which can be used as high-capacity anodes are also received much interest recently. Because of the multivalent variation property of vanadium, vanadium-based anode materials show great potential to realize a high capacity with the valence of vanadium reduced to +3, +2 or even lower. Till now, considerable amount of vanadium-based materials have been investigated about their electrochemical properties as LIB anodes, including V_2O_3 [198], Li_3VO_4 [31], CaV_4O_9 [34], $VOPO_4$ [199], VS_4 [32], VN [200], *etc*. Based on the present advances, here we mainly discuss the progresses of Li_3VO_4 and VS_4 as they show higher potential toward practical application in the near future regarding their electrochemical properties.

4.1. Li_3VO_4

Li_3VO_4 is a newly identified LIB anode based on intercalation reaction, which attracted considerable interests in recent years since the first report by Li et al., in 2013 [31]. Before used as a LIB anode, this phase has been investigated as the optic materials and ionic conduction materials for a long time. Li_3VO_4 is isostructural to Li_3PO_4 and has the feature of high lithium diffusion mobility (4×10^{-5} S cm^{-1}). But it suffers from low electronic conductivity. In the first investigation of this material as a LIB anode, Li_3VO_4 was prepared by a solid-state method, and a reversible capacity of ~323 mAh g^{-1} can be achieved, comparable to that of commercial graphite. Besides, galvanostatic intermittent titration technique (GITT) measurement revealed the maximum specific capacity of 394 mAh g^{-1}, corresponding to two Li^+ intercalation per formula. More importantly, the delivered capacity was mainly at a voltage range of 0.5–1.0 V vs. Li^+/Li (Fig. 12a). Compared with the other two typical intercalation-based anodes, graphite (capacity of ~370 mAh g^{-1} with an average lithiation voltage of ~0.1 V) and $Li_4Ti_5O_{12}$ (capacity of ~160 mAh g^{-1} with an average lithiation voltage of ~1.6 V), Li_3VO_4 has a distinct trade-off in the energy density and safety. Based on the reversible capacity and average voltage, the energy density of Li_3VO_4 was calculated to be 2.5 times of that of $Li_4Ti_5O_{12}$ (Fig. 12a). Even though it is lower than that of graphite (3.6 times of $Li_4Ti_5O_{12}$), the more suitable voltage of Li_3VO_4 means a better safety than graphite. This trade-off in energy density and safety is an important advantage of Li_3VO_4 when regards to practical application. The charge/discharge mechanism of Li_3VO_4 was also investigated through *ex situ* X-ray diffraction (XRD). In the initial discharge (lithium insertion) to 0.75 V, no distinct change was found in the XRD pattern. As the discharge continues, a new phase was clearly

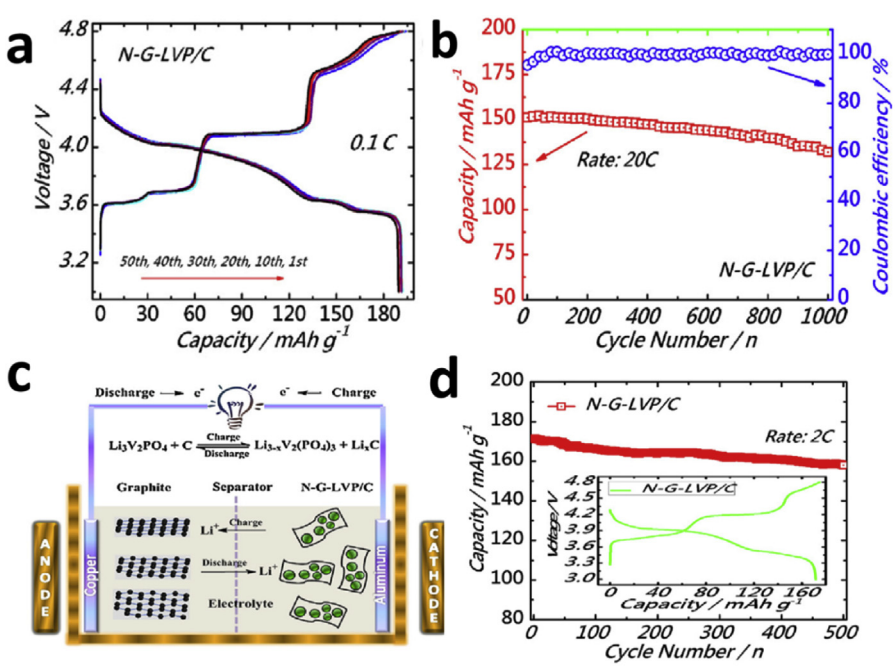

Fig. 11. (a) The charge-discharge profiles of nitrogen-doped graphene decorated LVP/C cathode in the voltage range of 3.0–4.8 V at 0.1 C. (b) The cycling performance of nitrogen-doped graphene decorated LVP/C cathode in the voltage range of 3.0–4.8 V at 20 C. (c) The illustration of full cell based on LVP as cathode and graphite as anode. (d) The cycling performance of the full cell at 2 C; the inset is the initial charge/discharge curve. Reproduced with permission from Elsevier [197]. LVP, $Li_3V_2(PO_4)_3$.

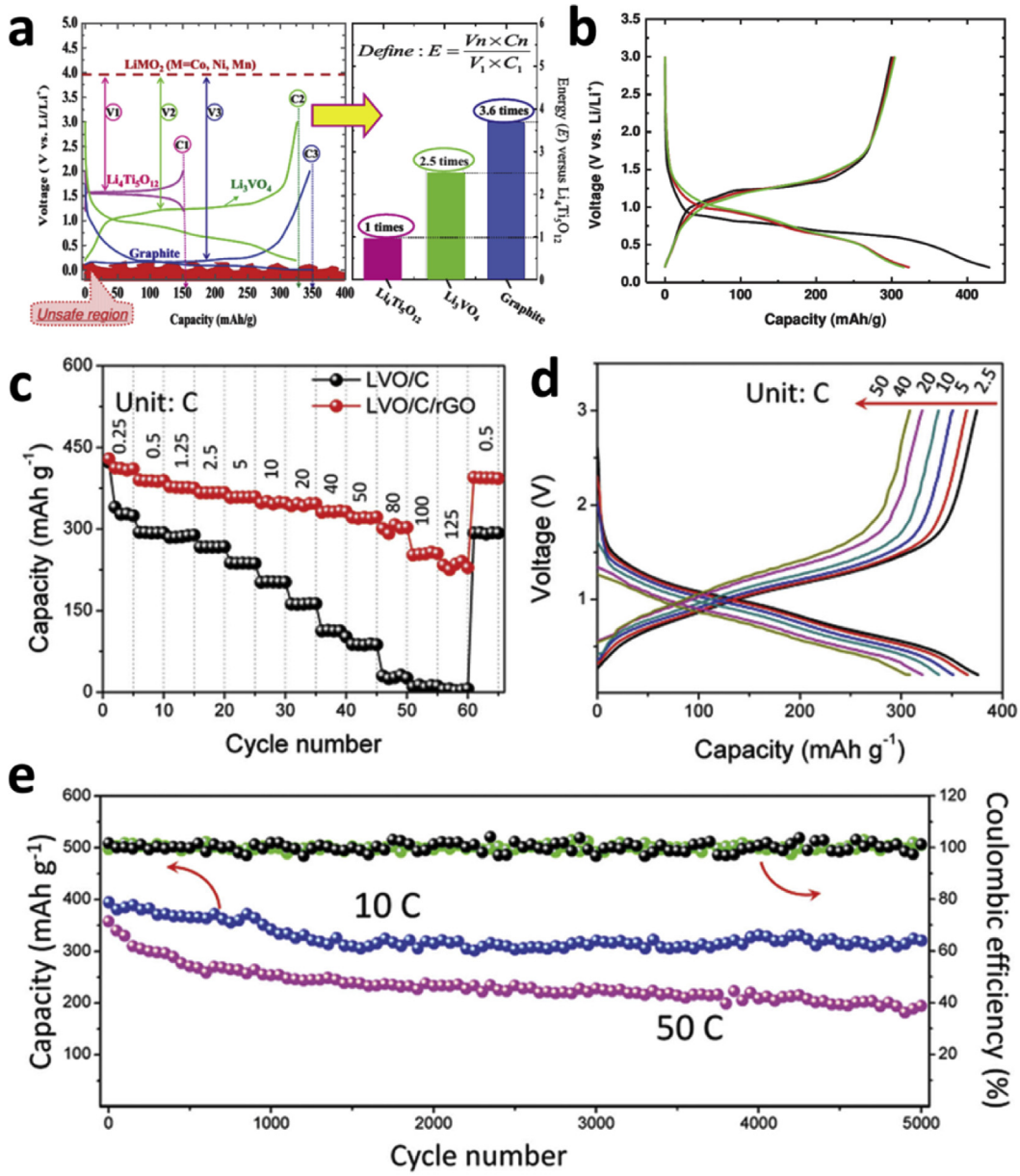

Fig. 12. (a) The potential, specific capacity and energy density of Li_3VO_4 compared with other two typical insertion-type anodes, $Li_4Ti_5O_{12}$ and graphite. (b) The charge/discharge profiles of Li_3VO_4 in initial three cycles. (c) Rate performance of mesoporous Li_3VO_4/C submicron-ellipsoids with and without rGO supporting. (d) The charge/discharge profiles of Li_3VO_4/C/rGO at different current rates. (e) The long-term cycling performance of Li_3VO_4/C/rGO. Reproduced with permission from (a–b) Ref. [31] and (c–e) Ref. [207] from Wiley VCH.

observed to grow up while the original phase weakened. Upon lithium extraction, a reversed transformation to the original state was detected by the XRD patterns. After charging to 3.0 V (fully lithium extraction), the phase totally came back to the original Li_3VO_4. Based on these results, a first solid-solution process and then a two-phase reaction mechanism were proposed for Li_3VO_4 during the Li^+ insertion. Also, these results indicate that the structure change of Li_3VO_4 is highly reversible upon lithium insertion/extraction [31].

Considering the energy density, safety and reversible lithium insertion/extraction property, Li_3VO_4 is a promising candidate for new LIB anode. However, the practical application still suffers from three challenges: the first is poor electric conductivity; the second is large voltage gap (~0.5 V) between charge and discharge (Fig. 12b); and the third is low initial coulombic efficiency (~70%) (Fig. 12b). Recent investigations and advances on Li_3VO_4 mainly center on resolving these three challenges.

In general, many electrode materials, both cathodes and anodes suffer from poor electric conductivity. The general ways to overcome this drawback are conductive coating/decoration together with nanostructure design, which increase the electric conductivity and shorten the ion/electron diffusion distance. In the case of Li_3VO_4, an important feature is that the valence of vanadium (+5) was demonstrated to be stable and cannot be reduced by residual carbon or reducing atmosphere even up to ~750 °C [201]. This ensures the realization of *in situ* carbon coating or other conductive decoration on Li_3VO_4 without damaging the crystal phase, which provides a broad space to improve the electrochemical performance. Liang et al. prepared carbon-coated Li_3VO_4 (Li_3VO_4/C) and presented a different understanding regarding to the theoretical

capacity and reaction mechanism of Li_3VO_4 [202]. They found that the initial discharge and charge capacities of Li_3VO_4/C can reach 738.5 and 547.1 mAh g^{-1}, respectively, which were much higher than those reported by Li et al. [31] where Li_3VO_4 was not coated with carbon. Through first-principles calculation and GITT measurement, the maximum intercalation amount of three Li^+ was proposed with the reduction of V^{5+} to V^{2+}, corresponding to a theoretical capacity of 590 mAh g^{-1}, which means a comparable energy density to the commercial graphite [202]. These results indicate the crucial role of conductive decoration on the electrochemical performance of Li_3VO_4. Therefore, it can be speculated that nanostructured Li_3VO_4 with conductive coating will exhibit much better lithium storage performance. Up to now, various Li_3VO_4 nanoarchitectures decorated with different conductive agents have been successively reported [203], such as Li_3VO_4 hollow microbox decorated with graphene nanosheets [204], hollow Li_3VO_4/carbon nanotube composite [205], carbon-encapsulated Li_3VO_4 [206], mesoporous Li_3VO_4/C submicron-ellipsoids supported on rGO [207], ultrathin Li_3VO_4 nanoribbon/graphene sandwich-like nanostructures [208] and MXene supported Li_3VO_4 [209] *etc*. All these reports demonstrated not only increased capacity but also enhanced cycling stability and rate capability. Especially, the mesoporous Li_3VO_4/C submicron-ellipsoids supported on rGO exhibited an ultrahigh rate capability (410 mAh g^{-1} at 0.25 C and 230 mAh g^{-1} at 125 C) and excellent long-term stability (retained 82.5% after 5000 cycles at 10 C) (Fig. 12c–e) [207].

Large voltage hysteresis is the other challenge for Li_3VO_4. As an intercalation reaction-based anode, it is still not very clear about the origin of the large voltage gap between charge and discharge. Li et al. proposed that the large voltage gap may be caused by its low electric conductivity [31]. But according to amounts of subsequent reports mentioned above, in which Li_3VO_4 was decorated by various conductive agents such as carbon, graphene, or carbon nanotubes, the voltage hysteresis seems not to be decreased distinctly, indicating that poor electric conductivity is not the only determinant. It should be noted that the large voltage hysteresis of conversion-type anodes (like transition metal oxides) was generally thought to be originated from the different reaction pathway between lithiation and delithiation [210]. Thus, it is safe to propose that the voltage gap of Li_3VO_4 between charge and discharge is related to the lithium insertion/extraction mechanism. Even though the phase variation of Li_3VO_4 has been investigated by *ex situ* XRD, the more detailed reaction process still needs to be further revealed to understand the origin of voltage gap.

About the low initial coulombic efficiency, the solid electrolyte interphase (SEI) formation was always regarded as one of the contributors to the observed irreversible capacity in the initial cycle. But it is not sure whether the low initial coulombic efficiency of Li_3VO_4 is related to the initial discharge/charge mechanism. Li et al. applied the *in situ* XRD technique to get deeper insights on the reaction mechanism of Li_3VO_4 and found the expanded d-spacing of (200) reflection after the initial discharge/charge cycle. It was proposed that this phenomenon may be the reason for the different discharge curves between the first and second cycles. Besides, the different reaction processes at different current rates were also observed. At a low rate of 0.2 C, a two phase transformation process was observed, while at a high rate of 1.0 C, the reflections was found to shift continually as the discharge/charge proceeded, indicating a non-equilibrium solid solution reaction mechanism [207]. The different reaction process is speculated to be another important factor that affects the initial coulombic efficiency at different rate. Note that a distinct increase of the initial coulombic efficiency to 94.0% was achieved for mesoporous Li_3VO_4/C/rGO [207], indicating that the good electron/ion transfer also has important impact on the initial reversibility. Besides, a surface-amorphous and oxygen-deficient $Li_3VO_{4-\delta}$ was also demonstrated to exhibit an increased initial coulombic efficiency. The increase was believed to be related to the improved charge transfer kinetics of $Li_3VO_{4-\delta}$ because of the amorphous surface [211].

Even though the practical application of Li_3VO_4 has been hindered by the abovementioned problems, its application prospect as a new LIB anode is still very optimistic considering the energy density and safety together with the achieved progress recent years. At present stage, fabricating composite electrodes like reported Li_3VO_4/graphite [212] or $Li_3VO_4/Li_4Ti_5O_{12}$ [213] nanocomposites to compensate for each other may be a good choice. Besides, apart from being used as an anode material for LIB independently, Li_3VO_4 was also regarded as a good coating material for surface modification because of its high ionic conductivity. When acting as a surface coating layer on the cathode materials such as $LiCoO_2$, $Li[Ni_{0.5}Co_{0.2}Mn_{0.3}]O_2$, $LiMnPO_4$, *etc*. [214–216], it was found that the electrodes exhibited improved capacity, cycling stability, and high rate capability, which was attributed to the stable protective effect and good Li^+ conduction of Li_3VO_4. This further broadens the application scope of Li_3VO_4 for LIBs.

4.2. VS_4

VS_4 has a special chain-like structure, as shown in Fig. 13a. The investigation about this kind of crystal structure in energy storage is rare in the past. The systematic study of VS_4 in energy storage begins from the work from Rout et al., in 2013 [32]. Even though the VS_4 mineral (patronite) was discovered as early as in 1906, the artificial synthesis of pure VS_4 phase was a challenge for a long period of time because of the existence of several non-stoichiometric vanadium sulfides phases and the experimental difficulties in controlling the sulfurization process with H_2S. Rout et al. successfully synthesized VS_4/rGO hybrids through a hydrothermal reaction [32]. They found that the addition of GO into the reaction mixture played a key role on the formation of VS_4 phase instead of VS_2, with the GO itself being reduced to rGO. When used as LIB anodes, the prepared VS_4/rGO hybrids displayed a high reversible capacity of 1066 mAh g^{-1} in the voltage range of 0.01–3.0 V. A distinct voltage plateau at about 2.0 V was observed (Fig. 13b). A capacity retention of 95% at 0.1 C after 100 cycles was obtained. These results demonstrated the potential of VS_4 as a new anode material for LIBs.

The impressive electrochemical performance of VS_4 further attracted interests about its electrochemical reaction mechanism. The Li^+ storage mechanism was investigated by Xu et al. afterward [217]. *Ex situ* transmission electron microscopy measurements and energy dispersive X-ray spectrometry mappings revealed that metallic V nanoparticles were generated in the discharge state (Fig. 13c) and remained in the charge state (Fig. 13d). The observations of metallic V suggested the conversion reaction of VS_4 during initial discharge process, while the metallic V was inert in the following charge process. The increased conductance of the electrode caused by the generated metallic V was manifested by the electrochemical impedance spectroscopy measurements. Based on the above results, together with ex situ XRD and CV results, the following reaction mechanism was proposed:

The initial discharge process:

$$VS_4 + 3Li^+ + 3e^- \rightarrow Li_3VS_4 \text{ (above 1.7 V)}$$

$$Li_3VS_4 + 5Li^+ + 5e^- \rightarrow 4Li_2S + V \text{ (0.01 V)}$$

The subsequent cycles:

$$Li_2S \leftrightarrow S + 2Li^+ + 2e^- \text{ (below 3 V)}$$

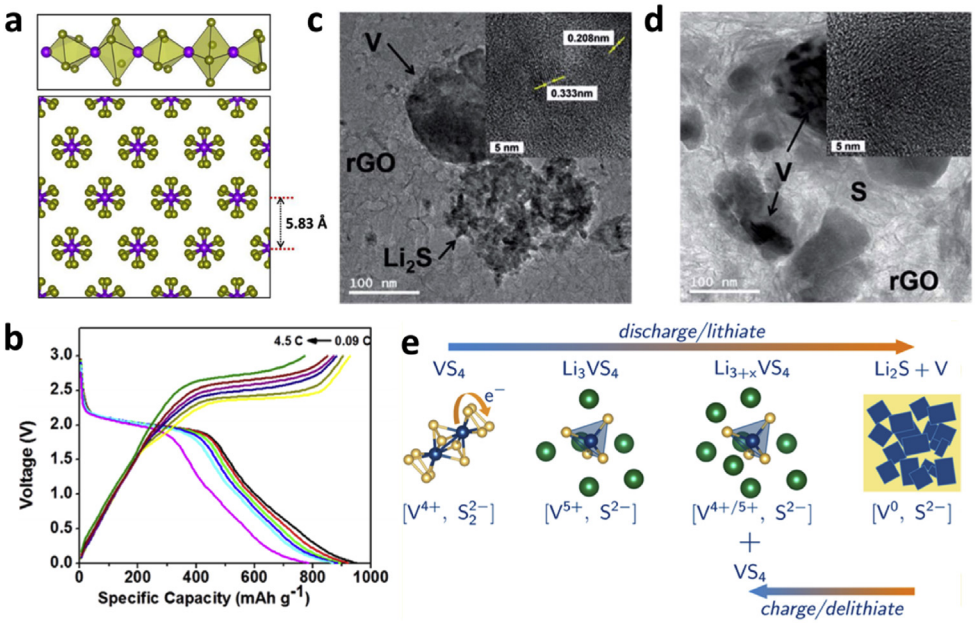

Fig. 13. (a) Schematic illustration of the chain-like structure of VS_4. (b) Charge/discharge profiles of VS_4 for Li storage at different current rates within 0.01–3.0 V. (c) *Ex situ* transmission electron microscopy (TEM) image of the VS_4 electrode at fully discharged state. (d) *Ex situ* TEM image of the VS_4 electrode at fully charged state. (e) Schematic illustration of the reaction mechanism of VS_4 in initial discharge process. Reproduced with permission from (a–b) American Chemical Society [32], (c–d) The Royal Society of Chemistry [217] and (e) American Chemical Society [218].

Such a mechanism was further confirmed and elucidated by Britto et al. using several short-range characterization tools including magnetic resonance spectroscopy and X-ray absorption near edge spectroscopy [218]. Note that the initial discharge process involves a complex redox interplay with electron transfer between the cation and anion. The initial lithiation leads to an electron transfer from V^{4+} to S_2^{2-}, resulting in the formation of V^{5+} and S^{2-} to form Li_3VS_4. The further lithiation is accompanied by the reduction of V^{5+} to firstly form a mixed valent compound $Li_{3+x}VS_4$, and finally to metallic vanadium and Li_2S (Fig. 13e). Such a complex redox reaction mechanism is different from most electrode materials where electron transfer is only centered on the cation or on the anion. In the other side, it can be found that the reaction is similar to that in Li-S batteries in subsequent cycles. Based on the proposed Li storage mechanism, a theoretical capacity of 1196 mAh g^{-1} can be calculated based on eight Li^+ storage, which is close to the achieved first charge capacity of 1170 mAh g^{-1}. Note that metallic vanadium was generated for VS_4 when discharged to 0.01 V, which is different from the electrochemical behavior of vanadium-based oxides in low voltage where the valence of vanadium cannot be reduced to zero. The difference can be ascribed to the stronger bond strength of V-O bonds than that of V-S bonds.

5. Summary and outlook

Next-generation lithium-based batteries require higher energy density to meet the development of electric vehicles and other electronic devices. The research about multi-electron reaction electrodes is very significant for realizing higher energy density. Vanadium-based electrode materials is a very important group for multi-electron reaction. This review focused on the typical vanadium-based materials including V_2O_5, VO_2, LiV_3O_8, $VOPO_4$, $LiVOPO_4$, $Li_3V_2(PO_4)_3$, Li_3VO_4, and VS_4 and discussed their structure, electrochemical performance, reaction/degradation mechanism, and optimization strategies in the case of multilithium intercalation/deintercalation. With the ability for multilithium insertion/extraction, these phases exhibit much higher capacity than the present commercialized electrode system. However, structure degradation and fast capacity fading are general challenges suffered by these phases during the multilithium reaction. Nanostructure design coordinated with conductive decoration, surface modification, or metal ions doping is the most popular way to enhance the cycling stability. In the other sides, controlling the lithium intercalation amount by narrowing the voltage range is also an effective way to improve the cycling stability but accompanied with the sacrifice of capacity. Improving the cycling stability at wider voltage range for multilithium reaction without sacrifice in capacity is still a key research direction for these vanadium-based electrodes in the future.

Future directions about these vanadium-based multi-electron reaction electrodes include in our viewpoints: (1) obtaining deeper insights about the degradation mechanism in the case of multilithium reaction at wide voltage range. Even though the phase evolution and degradation mechanism of V_2O_5 have been clearly revealed, those for other materials such as VO_2, $VOPO_4$ and $Li_3V_2(PO_4)_3$ have not been fully understood. More detailed understanding is required through advanced characterization techniques, such as *in situ* characterization, which will help to find the better optimization strategies. (2) Achieving more effective and efficient optimization strategies. Even though some works have reported impressive results with both high capacity and good cycling performance, the applied synthesis methods and optimization strategies are relatively complex and not benefit to commercialization. It will be always an important direction to achieve better performance with simpler strategies. (3) Evaluating the potential of these phases in full cells coupled with lithium metal anode. Except $Li_3V_2(PO_4)_3$ and $LiVOPO_4$, the other vanadium-based cathodes with multi-electron reaction are all Li-poor electrodes, which suggests that coupled with lithium metal anode is the ultimate way for their practical application. Considering that both the cathode and anode show a high capacity in such systems (such as V_2O_5//Li, LiV_3O_8//Li, $VOPO_4$//Li), it is attractive to see what level can the energy density

reach in such systems. Attempts in this direction are very significant to realize the practical application of vanadium-based multi-electron reaction electrode materials and promote the innovation of battery technology in the years to come.

Declaration of competing interest

The authors declare that they have no known competing financial interests or personal relationships that could have appeared to influence the work reported in this paper.

Acknowledgment

This work was supported by the National Natural Science Fund for Distinguished Young Scholars (51425204), the National Natural Science Foundation of China (51832004, 51521001), the National Key Research and Development Program of China (2016YFA0202601), the Programme of Introducing Talents of Discipline to Universities (B17034), the Yellow Crane Talent (Science & Technology) Program of Wuhan City, State Key Laboratory of Advanced Technology for Materials Synthesis and Processing (WUT: 2019-KF-2, 2019-KF-5).

References

[1] M. Winter, et al., Before Li ion batteries, Chem. Rev. 118 (2018) 11433–11456.
[2] S. Chu, et al., The path towards sustainable energy, Nat. Mater. 16 (2016) 16–22.
[3] J.F. Peters, et al., Life cycle assessment of sodium-ion batteries, Energy Environ. Sci. 9 (2016) 1744–1751.
[4] A.W. Golubkov, et al., Thermal-runaway experiments on consumer Li-ion batteries with metal-oxide and olivin-type cathodes, RSC Adv. 4 (2013) 3633–3642.
[5] P.G. Bruce, et al., Nanomaterials for rechargeable lithium batteries, Angew. Chem. 47 (2008) 2930–2946.
[6] D. Bruce, et al., Electrical energy storage for the grid: a battery of choices, Science 334 (2011) 928–935.
[7] J.B. Goodenough, Y. Kim, Challenges for rechargeable Li batteries, Chem. Mater. 22 (2010) 587–603.
[8] P.G. Bruce, et al., Li-O_2 and Li-S batteries with high energy storage, Nat. Mater. 11 (2012) 19–29.
[9] U.S. Department of Energy, Quadrennial Technology Review, 2015. https://energy.gov/sites/prod/files/2017/03/f34/quadrennial-technology-review-2015_1.pdf.
[10] M.S. Whittingham, et al., Can multielectron intercalation reactions Be the basis of next generation batteries, Acc. Chem. Res. 51 (2018) 258–264.
[11] F. Wu, et al., Multi-electron reaction materials for sodium-based batteries, Mater. Today 21 (2018) 960–973.
[12] R. Chen, et al., Advanced high energy density secondary batteries with multi-electron reaction materials, Adv. Sci. 3 (2016), 1600051.
[13] N.A. Chernova, et al., Layered vanadium and molybdenum oxides: batteries and electrochromics, J. Mater. Chem. 19 (2009) 2526–2552.
[14] Y. Yuan, L. Hong, Micro-and nano-structured vanadium pentoxide (V_2O_5) for electrodes of lithium-ion batteries, Adv. Energy Mater. 7 (2017), 1602545.
[15] M. Liu, et al., Recent advances in nanostructured vanadium oxides and composites for energy conversion, Adv. Energy Mater. 7 (2017), 1700885.
[16] M. Ulaganathan, et al., Recent advancements in all-vanadium redox flow batteries, Adv. Mater. Interfaces 3 (2016), 1500309.
[17] J. Yao, et al., Revitalized interest in vanadium pentoxide as cathode material for lithium-ion batteries and beyond, Energy Storage Mater. 11 (2018) 205–259.
[18] C. Liu, et al., A promising cathode for Li-ion batteries: $Li_3V_2(PO_4)_3$, Energy Storage Mater. 4 (2016) 15–58.
[19] M.S. Whittingham, The role of ternary phases in cathode reactions, J. Electrochem. Soc. 123 (1976) 315–320.
[20] K.J. Takeuchi, et al., Silver vanadium oxides and related battery applications, Coord. Chem. Rev. 219 (2001) 283–310.
[21] E.S. Takeuchi, P. Piliero, Lithium/silver vanadium oxide batteries with various silver to vanadium ratios, J. Power Sources 21 (1987) 133–141.
[22] R.P. Ramasamy, et al., Discharge characteristics of silver vanadium oxide cathodes, J. Appl. Electrochem. 36 (2006) 487–497.
[23] R.A. Leising, et al., Solid-state characterization of reduced silver vanadium oxide from the Li/SVO discharge reaction, Inorg. Chem. 33 (1994) 5733–5740.
[24] E.M. Sorensen, et al., $Ag_4V_2O_6F_2$: an electrochemically active and high silver density phase, J. Am. Chem. Soc. 127 (2005) 6347–6352.
[25] F. Sauvage, et al., $Ag_4V_2O_6F_2$ (SVOF): a high silver density phase and potential new cathode material for implantable cardioverter defibrillators, Inorg. Chem. 47 (2008) 8464–8472.
[26] H. Ma, et al., α-CuV_2O_6 nanowires: hydrothermal synthesis and primary lithium battery application, J. Am. Chem. Soc. 39 (2008) 5361–5367.
[27] F. Cheng, J. Chen, Transition metal vanadium oxides and vanadate materials for lithium batteries, J. Mater. Chem. 21 (2011) 9841–9848.
[28] D. Lin, et al., Reviving the lithium metal anode for high-energy batteries, Nat. Nanotechnol. 12 (2017) 194–206.
[29] P. Liu, et al., Recent progress in the applications of vanadium-based oxides on energy storage: from low-dimensional nanomaterials synthesis to 3D micro/nano-structures and free-standing electrodes fabrication, Adv. Energy Mater. 7 (2017), 1700547.
[30] G. Yang, et al., 3D hierarchical AlV_3O_9 microspheres: first synthesis, excellent lithium ion cathode properties, and investigation of electrochemical mechanism, Nano Energy 15 (2015) 281–292.
[31] H. Li, et al., Li_3VO_4: a promising insertion anode material for lithium-ion batteries, Adv. Energy Mater. 3 (2013) 428–432.
[32] C.S. Rout, et al., Synthesis and characterization of patronite form of vanadium sulfide on graphitic layer, J. Am. Chem. Soc. 135 (2013) 8720–8725.
[33] W. Fang, et al., Facile hydrothermal synthesis of VS_2/graphene nanocomposites with superior high-rate capability as lithium-ion battery cathodes, ACS Appl. Mater. Interfaces 7 (2015) 13044–13052.
[34] X. Xu, et al., Realizing stable lithium and sodium storage with high areal capacity using novel nanosheet-assembled compact CaV_4O_9 microflowers, Nano Energy 50 (2018) 606–614.
[35] D.W. Su, et al., Hierarchical orthorhombic V_2O_5 hollow nanospheres as high performance cathode materials for sodium-ion batteries, J. Mater. Chem. A 2 (2014) 11185–11194.
[36] H.T. Tan, et al., Vanadium-based nanostructure materials for secondary lithium battery applications, Nanoscale 7 (2015) 14595–14607.
[37] X. Huang, et al., Vanadium pentoxide-based cathode materials for lithium-ion batteries: morphology control, carbon hybridization, and cation doping, Part. Part. Syst. Charact. 32 (2015) 276–294.
[38] C. Delmas, et al., The $Li_xV_2O_5$ system: an overview of the structure modifications induced by the lithium intercalation, Solid State Ion. 69 (1994) 257–264.
[39] S.H. Ng, et al., Flame spray-pyrolyzed vanadium oxide nanoparticles for lithium battery cathodes, Phys. Chem. Chem. Phys. 11 (2009) 3748–3755.
[40] A. Pan, et al., Facile synthesized nanorod structured vanadium pentoxide for high-rate lithium batteries, J. Mater. Chem. 20 (2010) 9193–9199.
[41] L. Mai, et al., Electrospun ultralong hierarchical vanadium oxide nanowires with high performance for lithium ion batteries, Nano Lett. 10 (2010) 4750–4755.
[42] Q. An, et al., Supercritically exfoliated ultrathin vanadium pentoxide nanosheets with high rate capability for lithium batteries, Phys. Chem. Chem. Phys. 15 (2013) 16828–16833.
[43] T. Zhai, et al., Centimeter-long V_2O_5 nanowires: from synthesis to field-emission, electrochemical, electrical transport, and photoconductive properties, Adv. Mater. 22 (2010) 2547–2552.
[44] K.H. Seng, et al., Free-standing V_2O_5 electrode for flexible lithium ion batteries, Electrochem. Commun. 13 (2011) 383–386.
[45] W. Cheng, et al., Design of vanadium oxide core–shell nanoplatelets for lithium ion storage, J. Mater. Chem. A 3 (2015) 2861–2868.
[46] M. Qin, et al., Template-free synthesis of vanadium oxides nanobelt arrays as high-rate cathode materials for lithium ion batteries, J. Power Sources 268 (2014) 700–705.
[47] S. Liang, et al., Template-free synthesis of ultra-large V_2O_5 nanosheets with exceptional small thickness for high-performance lithium-ion batteries, Nano Energy 13 (2015) 58–66.
[48] X. Rui, et al., Ambient dissolution–recrystallization towards large-scale preparation of V_2O_5 nanobelts for high-energy battery applications, Nano Energy 22 (2016) 583–593.
[49] X. Rui, et al., Ultrathin V_2O_5 nanosheet cathodes: realizing ultrafast reversible lithium storage, Nanoscale 5 (2013) 556–560.
[50] H. Xu, et al., Substrate-free fabrication of self-supported V_2O_5 nanobelt arrays by a low-temperature solvothermal method with high electrochemical performance, Nanotechnology 27 (2016), 315402.
[51] P. Zhang, et al., A high-rate V_2O_5 hollow microclew cathode for an all-vanadium-based lithium-ion full cell, Small 12 (2016) 1082–1090.
[52] A. Pan, et al., Synthesis of hierarchical three-dimensional vanadium oxide microstructures as high-capacity cathode materials for lithium-ion batteries, ACS Appl. Mater. Interfaces 4 (2012) 3874–3879.
[53] A.Q. Pan, et al., Uniform V_2O_5 nanosheet-assembled hollow microflowers with excellent lithium storage properties, Energy Environ. Sci. 6 (2013) 1476–1479.
[54] G. Li, et al., Synthesis of V_2O_5 hierarchical structures for long cycle-life lithium-ion storage, J. Mater. Chem. A 3 (2015) 1103–1109.
[55] L. Chen, et al., Hierarchical vanadium pentoxide microflowers with excellent long-term cyclability at high rates for lithium ion batteries, J. Power Sources 272 (2014) 991–996.
[56] M.M. Rahman, et al., Self-assembled V_2O_5 interconnected microspheres produced in a fish-water electrolyte medium as a high-performance lithium-ion-battery cathode, Nano Res. 8 (2015) 3591–3603.

[57] Q. An, et al., Top-down fabrication of three-dimensional porous V_2O_5 hierarchical microplates with tunable porosity for improved lithium battery performance, J. Mater. Chem. A 2 (2014) 3297–3302.
[58] L. Mai, et al., Nanoflakes-assembled three-dimensional hollow-porous V_2O_5 as lithium storage cathodes with high-rate capacity, Small 10 (2014) 3032–3037.
[59] Q. An, et al., Three-dimensional porous V_2O_5 hierarchical octahedrons with adjustable pore architectures for long-life lithium batteries, Nano Res. 8 (2015) 481–490.
[60] Q. An, et al., Three-dimensional interconnected vanadium pentoxide nanonetwork cathode for high-rate long-life lithium batteries, Small 11 (2015) 2654–2660.
[61] H.B. Wu, et al., Template-assisted formation of rattle-type V_2O_5 hollow microspheres with enhanced lithium storage properties, Adv. Funct. Mater. 23 (2013) 5669–5674.
[62] H. Pang, et al., Template-free bottom-up synthesis of yolk-shell vanadium oxide as high performance cathode for lithium ion batteries, Chem. Commun. 49 (2013) 1536–1538.
[63] Q. Yue, et al., Mesoporous single-crystalline V_2O_5 nanorods assembled into hollow microspheres as cathode materials for high-rate and long-life lithium-ion batteries, Chem. Commun. 50 (2014) 13362–13365.
[64] S. Wang, et al., Three-dimensional porous V_2O_5 cathode with ultra high rate capability, Energy Environ. Sci. 4 (2011) 2854.
[65] C. Zhang, et al., Additive-free synthesis of 3D porous V_2O_5 hierarchical microspheres with enhanced lithium storage properties, Energy Environ. Sci. 6 (2013) 974–978.
[66] F. Guo, et al., Precursor-mediated synthesis of double-shelled V_2O_5 hollow nanospheres as cathode material for lithium-ion batteries, CrystEngComm 18 (2015) 4068–4073.
[67] H. Song, et al., Facile synthesis of mesoporous V_2O_5 nanosheets with superior rate capability and excellent cycling stability for lithium ion batteries, J. Power Sources 294 (2015) 1–7.
[68] M. Chen, et al., Free-standing three-dimensional continuous multilayer V_2O_5 hollow sphere arrays as high-performance cathode for lithium batteries, J. Power Sources 288 (2015) 145–149.
[69] Y.N. Ko, et al., A new strategy for synthesizing yolk-shell V_2O_5 powders with low melting temperature for high performance Li-ion batteries, Nanoscale 5 (2013) 8899–8903.
[70] C. Zhang, et al., Template-free synthesis of highly porous V_2O_5 cuboids with enhanced performance for lithium ion batteries, Nanotechnology 27 (2016), 305404.
[71] J. Wang, et al., Multi-shelled metal oxides prepared via an anion-adsorption mechanism for lithium-ion batteries, Nat. Energy 1 (2016) 16050.
[72] X.-F. Zhang, et al., Carbon-coated V_2O_5 nanocrystals as high performance cathode material for lithium ion batteries, Chem. Mater. 23 (2011) 5290–5292.
[73] G.X. Pan, et al., Carbon cloth supported vanadium pentaoxide nanoflake arrays as high-performance cathodes for lithium ion batteries, Electrochim. Acta 149 (2014) 349–354.
[74] M. Ihsan, et al., V_2O_5/mesoporous carbon composite as a cathode material for lithium-ion batteries, Electrochim. Acta 173 (2015) 172–177.
[75] C. Han, et al., V_2O_5 quantum dots/graphene hybrid nanocomposite with stable cyclability for advanced lithium batteries, Nano Energy 2 (2013) 916–922.
[76] S.H. Choi, Y.C. Kang, Uniform decoration of vanadium oxide nanocrystals on reduced graphene-oxide balls by an aerosol process for lithium-ion battery cathode material, Chem. Eur J. 20 (2014) 6294–6299.
[77] H. Liu, W. Yang, Ultralong single crystalline V_2O_5 nanowire/graphene composite fabricated by a facile green approach and its lithium storage behavior, Energy Environ. Sci. 4 (2011) 4000–4008.
[78] J. Cheng, et al., Self-assembled V_2O_5 nanosheets/reduced graphene oxide hierarchical nanocomposite as a high-performance cathode material for lithium ion batteries, J. Mater. Chem. A 1 (2013) 10814–10820.
[79] H. Zhao, et al., Vanadium oxides–reduced graphene oxide composite for lithium-ion batteries and supercapacitors with improved electrochemical performance, J. Power Sources 222 (2013) 21–31.
[80] H.J. Song, et al., Enhanced lithium storage in reduced graphene oxide-supported M-phase vanadium (IV) dioxide nanoparticles, Sci. Rep. 6 (2016) 30202.
[81] D. Chen, et al., Reduced graphene oxide enwrapped vanadium pentoxide nanorods as cathode materials for lithium-ion batteries, Phys. E 56 (2014) 231–237.
[82] B. Yan, et al., Crumpled reduced graphene oxide conformally encapsulated hollow V_2O_5 nano/microsphere achieving brilliant lithium storage performance, Nano Energy 24 (2016) 32–44.
[83] R. Yu, et al., Facile synthesis of hierarchical networks composed of highly interconnected V_2O_5 nanosheets assembled on carbon nanotubes and their superior lithium storage properties, ACS Appl. Mater. Interfaces 5 (2013) 12394–12399.
[84] D. Kong, et al., Encapsulating V_2O_5 into carbon nanotubes enables the synthesis of flexible high-performance lithium ion batteries, Energy Environ. Sci. 9 (2016) 906–911.
[85] M. Xie, et al., Stabilizing an amorphous V_2O_5/carbon nanotube paper electrode with conformal TiO_2 coating by atomic layer deposition for lithium ion batteries, J. Mater. Chem. A 4 (2016) 537–544.
[86] J. Cheng, et al., Synthesis of a porous sheet-like V_2O_5–CNT nanocomposite using an ice-templating 'bricks-and-mortar' assembly approach as a high-capacity, long cycle life cathode material for lithium-ion batteries, J. Mater. Chem. A 4 (2016) 2729–2737.
[87] Z. Cao, B. Wei, V_2O_5/single-walled carbon nanotube hybrid mesoporous films as cathodes with high-rate capacities for rechargeable lithium ion batteries, Nano Energy 2 (2013) 481–490.
[88] X. Wei, et al., A Bowknot-like RuO_2 quantum dots@V_2O_5 cathode with largely improved electrochemical performance, Phys. Chem. Chem. Phys. 16 (2014) 18680–18685.
[89] C. Niu, et al., Three dimensional V_2O_5/NaV_6O_{15} hierarchical heterostructures: controlled synthesis and synergistic effect investigated by in situ X-ray diffraction, Nano Energy 27 (2016) 147–156.
[90] J. Yan, et al., V_2O_5 loaded on SnO_2 nanowires for high-rate li ion batteries, Adv. Mater. 23 (2011) 746–750.
[91] S. Tian, et al., Enhanced cycling stability of TiO_2-coated V_2O_5 nanorods through a surface sol–gel process for lithium ion battery applications, J. Mater. Chem. A 2 (2014) 2896–2900.
[92] D.-J. Yan, et al., Facile and elegant self-organization of Ag nanoparticles and TiO_2 nanorods on V_2O_5 nanosheets as a superior cathode material for lithium-ion batteries, J. Mater. Chem. A 4 (2016) 4900–4907.
[93] H. Xu, et al., Fabricating SiO_2-coated V_2O_5 nanoflake arrays for high-performance lithium-ion batteries with enhanced cycling capability, J. Mater. Chem. A 4 (2016) 4098–4106.
[94] L. Mai, et al., Cucumber-like V_2O_5/poly(3,4-ethylenedioxythiophene)&MnO_2 nanowires with enhanced electrochemical cyclability, Nano Lett. 13 (2013) 740–745.
[95] D. Chao, et al., A V_2O_5/conductive-polymer core/shell nanobelt array on three-dimensional graphite foam: a high-rate, ultrastable, and free-standing cathode for lithium-ion batteries, Adv. Mater. 26 (2014) 5794–5800.
[96] L. Noerochim, et al., Impact of mechanical bending on the electrochemical performance of bendable lithium batteries with paper-like free-standing V_2O_5–polypyrrole cathodes, J. Mater. Chem. 22 (2012) 11159–11165.
[97] X. Peng, et al., Hydrogenated V_2O_5 nanosheets for superior lithium storage properties, Adv. Funct. Mater. 26 (2016) 784–791.
[98] H. Zeng, et al., Nanostructured Mn-doped V_2O_5 cathode material fabricated from layered vanadium jarosite, Chem. Mater. 27 (2015) 7331–7336.
[99] K. Zhu, et al., Synergetic effects of Al^{3+} doping and graphene modification on the electrochemical performance of V_2O_5 cathode materials, ChemSusChem 8 (2015) 1017–1025.
[100] C. Peng, et al., Carbon-encapsulated Mn-doped V_2O_5 nanorods with long span life for high-power rechargeable lithium batteries, Electrochim. Acta 192 (2016) 216–226.
[101] Y.-Z. Zheng, et al., Nickel-mediated polyol synthesis of hierarchical V_2O_5 hollow microspheres with enhanced lithium storage properties, J. Mater. Chem. A 3 (2015) 1979–1985.
[102] H. Song, et al., Self-doped V^{4+}–V_2O_5 nanoflake for 2 Li-ion intercalation with enhanced rate and cycling performance, Nano Energy 22 (2016) 1–10.
[103] H. Yu, et al., Cu doped V_2O_5 flowers as cathode material for high-performance lithium ion batteries, Nanoscale 5 (2013) 4937–4943.
[104] Z.-l. Wang, et al., Facile and low-cost synthesis of large-area pure V_2O_5 nanosheets for high-capacity and high-rate lithium storage over a wide temperature range, ChemPlusChem 77 (2012) 124–128.
[105] H.E. Wang, et al., Facile synthesis of hierarchical and porous V_2O_5 microspheres as cathode materials for lithium ion batteries, J. Colloid Interface Sci. 418 (2014) 74–80.
[106] Q. Song, et al., Fabrication of nanostructured V_2O_5 via urea combustion for high-performance Li-ion battery cathode, RSC Adv. 5 (2015) 4256–4260.
[107] Z. Tong, et al., Novel morphology changes from 3D ordered macroporous structure to V_2O_5 nanofiber grassland and its application in electrochromism, Sci. Rep. 5 (2015) 16864.
[108] J.-K. Lee, et al., Electrodeposition of mesoporous V_2O_5 with enhanced lithium-ion intercalation property, Electrochem. Commun. 11 (2009) 1571–1574.
[109] D. Yu, et al., Mesoporous vanadium pentoxide nanofibers with significantly enhanced Li-ion storage properties by electrospinning, Energy Environ. Sci. 4 (2011) 858–861.
[110] Y.L. Cheah, et al., Improved elevated temperature performance of Al-intercalated V_2O_5 electrospun nanofibers for lithium-ion batteries, ACS Appl. Mater. Interfaces 4 (2012) 3270–3277.
[111] S. Zhan, et al., Structural and electrochemical properties of Al^{3+} doped V_2O_5 nanoparticles prepared by an oxalic acid assisted soft-chemical method, J. Alloy. Comp. 502 (2010) 92–96.
[112] S. Zhan, et al., Effects of Cr doping on the structural and electrochemical properties of V_2O_5, J. Alloy. Comp. 479 (2009) 652–656.
[113] D.M. Yu, et al., Effect of manganese doping on Li-ion intercalation properties of V_2O_5 films, J. Mater. Chem. 20 (2010) 10841.
[114] S.-R. Li, et al., Three-dimensional porous $Fe_{0.1}V_2O_{5.15}$ thin film as a cathode material for lithium ion batteries, Electrochim. Acta 64 (2012) 81–86.
[115] Y. Li, et al., Sn-doped V_2O_5 film with enhanced lithium-ion storage performance, J. Phys. Chem. C 117 (2013) 23507–23514.
[116] G. Armstrong, et al., The synthesis and lithium intercalation electrochemistry of VO_2(B) ultra-thin nanowires, J. Power Sources 178 (2008) 723–728.

[117] C. Wu, Y. Xie, Promising vanadium oxide and hydroxide nanostructures: from energy storage to energy saving, Energy Environ. Sci. 3 (2010) 1191–1206.
[118] H. Liu, et al., Design and synthesis of a novel nanothorn VO_2(B) hollow microsphere and their application in lithium-ion batteries, J. Mater. Chem. 19 (2009) 2835.
[119] L. Zhang, et al., Mesoporous VO_2 nanowires with excellent cycling stability and enhanced rate capability for lithium batteries, RSC Adv. 4 (2014) 33332–33337.
[120] C. Niu, et al., VO_2 nanowires assembled into hollow microspheres for high-rate and long-life lithium batteries, Nano Lett. 14 (2014) 2873–2878.
[121] L. Mai, et al., Nanoscroll buffered hybrid nanostructural VO_2 (B) cathodes for high-rate and long-life lithium storage, Adv. Mater. 25 (2013) 2969–2973.
[122] Q. Zhao, et al., Facile synthesis of VO_2(B)/carbon nanobelts with high capacity and good cyclability, J. Power Sources 199 (2012) 350–354.
[123] X. Rui, et al., One-pot synthesis of carbon-coated VO_2(B) nanobelts for high-rate lithium storage, RSC Adv. 2 (2012) 1174–1180.
[124] C. Yan, et al., Stable lithium-ion cathodes from nanocomposites of VO_2 nanowires and CNTs, Nanotechnology 23 (2012), 475701.
[125] C. Nethravathi, et al., Hydrothermal synthesis of a monoclinic VO_2 nanotube–graphene hybrid for use as cathode material in lithium ion batteries, Carbon 50 (2012) 4839–4846.
[126] S. Yang, et al., Bottom-up approach toward single-crystalline VO_2-graphene ribbons as cathodes for ultrafast lithium storage, Nano Lett. 13 (2013) 1596–1601.
[127] C. Nethravathi, et al., N-doped graphene-VO_2(B) nanosheet-built 3D flower hybrid for lithium ion battery, ACS Appl. Mater. Interfaces 5 (2013) 2708–2714.
[128] G. Ren, et al., Vertically aligned VO_2(B) nanobelt forest and its three-dimensional structure on oriented graphene for energy storage, J. Mater. Chem. A 3 (2015) 10787–10794.
[129] D. Chao, et al., Graphene quantum dots coated VO_2 arrays for highly durable electrodes for Li and Na ion batteries, Nano Lett. 15 (2015) 565–573.
[130] M.S. Balogun, et al., Carbon quantum dot surface-engineered VO_2 interwoven nanowires: a flexible cathode material for lithium and sodium ion batteries, ACS Appl. Mater. Interfaces 8 (2016) 9733–9744.
[131] S. Li, et al., Carbon fiber cloth@VO_2(B): excellent binder-free flexible electrodes with ultrahigh mass-loading, J. Mater. Chem. A 4 (2016) 6426–6432.
[132] X. Zhou, et al., The synthesis, characterization and electrochemical properties of multi-wall carbon nanotube-induced vanadium oxide nanosheet composite as a novel cathode material for lithium ion batteries, Electrochim. Acta 74 (2012) 32–38.
[133] Y. Shi, et al., In-situ hydrothermal synthesis of graphene woven VO_2 nanoribbons with improved cycling performance, J. Power Sources 244 (2013) 684–689.
[134] Z. Fan, et al., Enhanced electrochemical performance of vanadium dioxide (B) nanoflowers with graphene nanoribbons support, RSC Adv. 6 (2016) 13297–13302.
[135] X. Xia, et al., VO_2 nanoflake arrays for supercapacitor and Li-ion battery electrodes: performance enhancement by hydrogen molybdenum bronze as an efficient shell material, Mater. Horiz. 2 (2015) 237–244.
[136] K. Nassau, D.W. Murphy, The quenching and electrochemical behavior of $Li_2O//V_2O_5$ glasses, J. Non-Cryst. Solids 44 (1981) 297–304.
[137] A. Pan, et al., Template free synthesis of LiV_3O_8 nanorods as a cathode material for high-rate secondary lithium batteries, J. Mater. Chem. 21 (2010) 1153–1161.
[138] H. Song, et al., High rate and stable Li-ion insertion in oxygen-deficient LiV_3O_8 nanosheets as a cathode material for lithium-ion battery, ACS Appl. Mater. Interfaces 9 (2017) 2875–2882.
[139] G.Q. Liu, et al., Study on the synthesis and properties of LiV_3O_8 rechargeable lithium batteries cathode, Electrochim. Acta 47 (2002) 3239–3243.
[140] A.M. Kannan, A. Manthiram, Low temperature synthesis and electrochemical behavior of LiV_3O_8 cathode, J. Power Sources 159 (2006) 1405–1408.
[141] K. Jin, et al., Lithium insertion behaviour of $Li_{1+x}V_3O_8$ with different degrees of crystallinity, J. Power Sources 81–82 (1999) 448–453.
[142] H. Liu, et al., Synthesis and electrochemical properties of single-crystalline LiV_3O_8 nanorods as cathode materials for rechargeable lithium batteries, J. Power Sources 192 (2009) 668–673.
[143] A. Pan, et al., Nanosheet-structured LiV_3O_8 with high capacity and excellent stability for high energy lithium batteries, J. Mater. Chem. 21 (2011) 10077–10084.
[144] X. Xu, et al., Topotactically synthesized ultralong LiV_3O_8 nanowire cathode materials for high-rate and long-life rechargeable lithium batteries, NPG Asia Mater. 4 (2012) e20.
[145] X. Lu, et al., Enhanced lithium ion transport by superionic pathways formed on the surface of two-dimensional structured $Li_{0.85}Na_{0.15}V_3O_8$ for high-performance lithium ion batteries, Electrochim. Acta 155 (2015) 148–156.
[146] S. Huang, et al., Enhanced electrochemical properties of Al_2O_3-coated LiV_3O_8 cathode materials for high-power lithium-ion batteries, J. Power Sources 245 (2014) 698–705.
[147] R. Mo, et al., Surface modification of LiV_3O_8 nanosheets via layer-by-layer self-assembly for high-performance rechargeable lithium batteries, J. Power Sources 257 (2014) 319–324.
[148] D. Sun, et al., Multi-layered $Al_2O_3/Li_xV_2O_5/LiV_3O_8$ nanoflakes with superior cycling stability as cathode material for Li-ion battery, Electrochim, Acta 157 (2015) 211–217.
[149] D. Sun, et al., $Li_xV_2O_5/LiV_3O_8$ nanoflakes with significantly improved electrochemical performance for Li-ion batteries, J. Mater. Chem. A 2 (2014) 8009–8016.
[150] R. Mo, et al., In situ synthesis of LiV_3O_8 nanorods on graphene as high rate-performance cathode materials for rechargeable lithium batteries, Chem. Commun. 49 (2013) 9143–9145.
[151] R. Mo, et al., Ultradispersed nanoarchitecture of LiV_3O_8 nanoparticle/reduced graphene oxide with high-capacity and long-life lithium-ion battery cathodes, Sci. Rep. 6 (2016) 19843.
[152] Z.K. Wang, et al., Graphene-nanosheet-wrapped LiV_3O_8 nanocomposites as high performance cathode materials for rechargeable lithium-ion batteries, J. Power Sources 307 (2016) 426–434.
[153] R. Mo, et al., Sandwich nanoarchitecture of LiV_3O_8/graphene multilayer nanomembranes via layer-by-layer self-assembly for long-cycle-life lithium-ion battery cathodes, J. Mater. Chem. A 3 (2015) 13717–13723.
[154] H. Guo, et al., Electrochemical characterization of polyaniline-LiV_3O_8 nanocomposite cathode material for lithium ion batteries, Electrochim. Acta 94 (2013) 113–123.
[155] J.H. Lee, et al., Electrochemical analysis of the effect of Cr coating the LiV_3O_8 cathode in a lithium ion battery with a lithium powder anode, ACS Appl. Mater. Interfaces 5 (2013) 7058–7064.
[156] H. Song, et al., Mo-doped LiV_3O_8 nanorod-assembled nanosheets as a high performance cathode material for lithium ion batteries, J. Mater. Chem. A 3 (2015) 3547–3558.
[157] H.Y. Xu, et al., Novel chemical method for synthesis of LiV_3O_8 nanorods as cathode materials for lithium ion batteries, Electrochim. Acta 49 (2004) 349–353.
[158] S. Liang, et al., LiV_3O_8/Ag composite nanobelts with enhanced performance as cathode material for rechargeable lithium batteries, J. Alloy. Comp. 583 (2014) 351–356.
[159] K. Yan, et al., Selective deposition and stable encapsulation of lithium through heterogeneous seeded growth, Nat. Energy 1 (2016) 16010.
[160] G. Zheng, et al., High performance lithium metal negative electrode with a soft and flowable polymer coating, ACS Energy Lett 1 (2016) 1247–1255.
[161] B.M. Azmi, et al., Vanadyl phosphates of $VOPO_4$ as a cathode of Li-ion rechargeable batteries, J. Power Sources 119–121 (2003) 273–277.
[162] Y.C. Lin, et al., Comparison of the polymorphs of $VOPO_4$ as multi-electron cathodes for rechargeable alkali-ion batteries, J. Mater. Chem. A 5 (2017) 17421–17431.
[163] C. Ling, et al., Phase stability and its impact on the electrochemical performance of $VOPO_4$ and $LiVOPO_4$, J. Mater. Chem. A 2 (2014) 12330–12339.
[164] C. Siu, et al., Enabling multi-electron reaction of ε-$VOPO_4$ to reach theoretical capacity for lithium-ion batteries, Chem. Commun. 54 (2018) 7802–7805.
[165] Z. Chen, et al., Electrochemical behavior of nanostructured ϵ-$VOPO_4$ over two redox plateaus, J. Electrochem. Soc. 160 (2013) A1777–A1780.
[166] Z. Chen, et al., A β-$VOPO_4$/ε-$VOPO_4$ composite Li-ion battery cathode, Electrochem. Commun. 46 (2014) 67–70.
[167] Y. Huang, et al., Thermal stability and reactivity of cathode materials for Li-ion batteries, ACS Appl. Mater. Interfaces 8 (2016) 7013–7021.
[168] B. Wen, et al., Molybdenum substituted vanadyl phosphate ε-$VOPO_4$ with enhanced two-electron transfer reversibility and kinetics for lithium-ion batteries, Chem. Mater. 28 (2016) 3159–3170.
[169] L. Wangoh, et al., Uniform second Li ion intercalation in solid state ε-$LiVOPO_4$, Appl. Phys. Lett. 109 (2016), 053904.
[170] Y.-C. Lin, et al., Thermodynamics, kinetics and structural evolution of ε-$LiVOPO_4$ over multiple lithium intercalation, Chem. Mater. 28 (2016) 1794–1805.
[171] K.L. Harrison, et al., Chemical and electrochemical lithiation of $LiVOPO_4$ cathodes for lithium-ion batteries, Chem. Mater. 26 (2014) 3849–3861.
[172] H. Zhou, et al., ε- and β-$LiVOPO_4$: phase transformation and electrochemistry, ACS Appl. Mater. Interfaces 9 (2017) 28537–28541.
[173] M. Francis, V. Hidalgo, et al., Rational synthesis and electrochemical performance of $LiVOPO_4$ polymorphs, J. Mater. Chem. A 7 (2019) 8423–8432.
[174] G. He, et al., Crystal chemistry of electrochemically and chemically lithiated layered α_I-$LiVOPO_4$, Chem. Mater. 27 (2015) 6699–6707.
[175] Y. Shi, et al., A high-performance solid-state synthesized $LiVOPO_4$ for lithium-ion batteries, Electrochem. Commun. 105 (2019) 106491.
[176] J. Rana, et al., Role of disorder in limiting the true multi-electron redox in ε-$LiVOPO_4$, J. Mater. Chem. A 6 (2018) 20669–20677.
[177] Y. Shi, et al., Electrochemical performance of nanosized disordered $LiVOPO_4$, ACS Omega 3 (2018) 7310–7323.
[178] N. Membreño, et al., Electrode/electrolyte interface of composite α-$Li_3V_2(PO_4)_3$ cathodes in a nonaqueous electrolyte for lithium ion batteries and the role of the carbon additive, Chem. Mater. 27 (2015) 3332–3340.
[179] S. Liang, et al., Carbon wrapped hierarchical $Li_3V_2(PO_4)_3$ microspheres for high performance lithium ion batteries, Sci. Rep. 6 (2016) 33682.
[180] Y. Cheng, et al., Phase-change enabled 2D $Li_3V_2(PO_4)_3$/C submicron sheets for advanced lithium-ion batteries, J. Power Sources 326 (2016) 203–210.
[181] L. Wang, et al., Structure tracking aided design and synthesis of $Li_3V_2(PO_4)_3$ nanocrystals as high-power cathodes for lithium ion batteries, Chem. Mater. 27 (2015) 5712–5718.

[182] X. Rui, et al., $Li_3V_2(PO_4)_3$ cathode materials for lithium-ion batteries: a review, J. Power Sources 258 (2014) 19–38.
[183] J. Gaubicher, et al., Rhombohedral form of $Li_3V_2(PO_4)_3$ as a cathode in Li-ion batteries, Chem. Mater. 32 (2000) 3240–3242.
[184] H. Huang, et al., Nanostructured composites: a high capacity, fast rate $Li_3V_2(PO_4)_3$/carbon cathode for rechargeable lithium batteries, Adv. Mater. 14 (2002) 1525–1528.
[185] Z. Jian, et al., NASICON-structured materials for energy storage, Adv. Mater. 29 (2017) 1601925.
[186] Y.Q. Qiao, et al., Synthesis and improved electrochemical performances of porous $Li_3V_2(PO_4)_3$/C spheres as cathode material for lithium-ion batteries, J. Power Sources 196 (2011) 7715–7720.
[187] Y. Jiang, et al., Graphene modified $Li_3V_2(PO_4)_3$ as a high-performance cathode material for lithium ion batteries, Electrochim. Acta 85 (2012) 377–383.
[188] Q. Chen, et al., Electrochemical performance of $Li_{3-x}Na_xV_2(PO_4)_3$/C composite cathode materials for lithium ion batteries, J. Power Sources 201 (2012) 267–273.
[189] J. Kang, et al., Pyro-synthesis of a high rate nano-$Li_3V_2(PO_4)_3$/C cathode with mixed morphology for advanced Li-ion batteries, Sci. Rep. 4 (2014) 4047.
[190] F. Teng, et al., Hydrothermal synthesis of plate-like carbon-coated $Li_3V_2(PO_4)_3$ and its low temperature performance for high power lithium ion batteries, Electrochim. Acta 91 (2013) 43–49.
[191] Y.Q. Qiao, et al., Synthesis of plate-like $Li_3V_2(PO_4)_3$/C as a cathode material for Li-ion batteries, J. Power Sources 196 (2011) 8706–8709.
[192] X. Zhang, et al., Ionic-liquid-Assisted synthesis of nanostructured and carbon-coated $Li_3V_2(PO_4)_3$ for high-power electrochemical storage devices, ChemSusChem 7 (2014) 1710–1718.
[193] C. Niu, et al., General synthesis of complex nanotubes by gradient electrospinning and controlled pyrolysis, Nat. Commun. 6 (2015) 7402.
[194] Y. Zhou, et al., Biochemistry-enabled 3D foams for ultrafast battery cathodes, ACS Nano 9 (2015) 4628–4635.
[195] X. Nan, et al., Highly efficient storage of pulse energy produced by triboelectric nanogenerator in $Li_3V_2(PO_4)_3$/C cathode Li-ion batteries, ACS Appl. Mater. Interfaces 8 (2016) 862–870.
[196] Y.Q. Qiao, et al., The low and high temperature electrochemical performances of $Li_3V_2(PO_4)_3$/C cathode material for Li-ion batteries, J. Power Sources 199 (2012) 287–292.
[197] K. Cui, et al., Nitrogen-doped graphene nanosheets decorated $Li_3V_2(PO_4)_3$/C nanocrystals as high-rate and ultralong cycle-life cathode for lithium-ion batteries, Electrochim. Acta 210 (2016) 45–52.
[198] C. Niu, et al., Carbon-supported and nanosheet-assembled vanadium oxide microspheres for stable lithium-ion battery anodes, Nano Res. 9 (2016) 128–138.
[199] B. Zhang, et al., $VOPO_4$ nanosheets as anode materials for lithium-ion batteries, Chem. Commun. 50 (2014) 11132–11134.
[200] L. Wang, et al., Hybrid 2D–0D graphene–VN quantum dots for superior lithium and sodium storage, Adv. Energy Mater. 6 (2016), 1502067.
[201] Z. Liang, et al., Synthesis of carbon-coated Li_3VO_4 and its high electrochemical performance as anode material for lithium-ion batteries, J. Power Sources 252 (2014) 244–247.
[202] Z. Liang, et al., New understanding of Li_3VO_4/C as potential anode for Li-ion batteries: preparation, structure characterization and lithium insertion mechanism, J. Power Sources 274 (2015) 345–354.
[203] S. Ni, et al., Vanadate-based materials for Li-ion batteries: the search for anodes for practical applications, Adv. Energy Mater. 9 (2019), 1803324.
[204] Y. Shi, et al., Hollow structured Li_3VO_4 wrapped with graphene nanosheets in situ prepared by a one-pot template-free method as an anode for lithium-ion batteries, Nano Lett. 13 (2016) 4715–4720.
[205] Q. Li, et al., A unique hollow Li_3VO_4/carbon nanotube composite anode for high rate long-life lithium-ion batteries, Nanoscale 6 (2014) 11072–11077.
[206] C. Zhang, et al., Fast and reversible Li ion insertion in carbon-encapsulated Li_3VO_4 as anode for lithium-ion battery, Adv. Funct. Mater. 25 (2015) 3497–3504.
[207] Q. Li, et al., Mesoporous Li_3VO_4/C submicron-ellipsoids supported on reduced graphene oxide as practical anode for high-power lithium-ion batteries, Adv. Sci. 2 (2015), 1500284.
[208] J. Liu, et al., Ultrathin Li_3VO_4 nanoribbon/graphene sandwich-like nanostructures with ultrahigh lithium ion storage properties, Nano Energy 12 (2015) 709–724.
[209] Y. Huang, et al., A safe and fast-charging lithium-ion battery anode using MXene supported Li_3VO_4, J. Mater. Chem. A 7 (2019) 11250–11256.
[210] J. Cabana, et al., Beyond intercalation-based Li-ion batteries: the state of the art and challenges of electrode materials reacting through conversion reactions, Adv. Energy Mater. 22 (2010) E170–E192.
[211] L. Chen, et al., Surface-amorphous and oxygen-deficient $Li_3VO_{4-\delta}$ as a promising anode material for lithium-ion batteries, Adv. Sci. 2 (2015), 1500090.
[212] S. Ni, et al., The electrochemical performance of lithium vanadate/natural graphite composite material as anode for lithium ion batteries, Electrochim. Acta 145 (2014) 327–334.
[213] Y. Sha, et al., One-pot combustion synthesis of Li_3VO_4-$Li_4Ti_5O_{12}$ nanocomposite as anode material of lithium-ion batteries with improved performance, Electrochim. Acta 222 (2016) 587–595.
[214] X. Pu, C. Yu, Enhanced overcharge performance of nano-$LiCoO_2$ by novel Li_3VO_4 surface coatings, Nanoscale 4 (2012) 6743–6747.
[215] Q. Fu, et al., Electrochemical performance and thermal stability of $Li_{1.18}Co_{0.15}Ni_{0.15}Mn_{0.52}O_2$ surface coated with the ionic conductor Li_3VO_4, J. Mater. Chem. A 2 (2014) 7555–7562.
[216] Y. Huang, et al., Improved cycle stability and high-rate capability of Li_3VO_4-coated $Li[Ni_{0.5}Co_{0.2}Mn_{0.3}]O_2$ cathode material under different voltages, J. Power Sources 256 (2014) 1–7.
[217] X. Xu, et al., Lithium reaction mechanism and high rate capability of VS_4-graphene nanocomposite as an anode material for lithium batteries, J. Mater. Chem. A 2 (2014) 10847–10853.
[218] S. Britto, et al., Multiple redox modes in the reversible lithiation of high-capacity, peierls-distorted vanadium sulfide, J. Am. Chem. Soc. 137 (2015) 8499–8508.